PFC/RR-86-25 DOE/ET-51013-207

SAFETY AND PROTECTION FOR LARGE SCALE SUPERCONDUCTING MAGNETS – FY1986 REPORT

R.J. Thome, M.M. Steeves, J.R. Hale, A.M. Dawson

December 1986

Plasma Fusion Center
Massachusetts Institute of Technology
Cambridge, Massachusetts 02139 USA

submitted to
Idaho National Engineering Laboratory
Idaho Falls, Idaho

Foreword

Much of the work reported herein was performed at the Kernforschungszentrum, Karlsruhe, FRG. The support, advice and assistance of K.P. Jüngst, G.W. Leppelmeier, P. Komarek, and members of the TESPE Team are acknowledged with thanks and appreciation.

Table of Contents

1 Introduction

The Fusion Program of the Future requires magnet systems which will store energy in the magnets at multigigajoule levels. The Compact Ignition Tokomak (CIT), for example, which will be the next step in the US fusion effort, is presently in a preconceptual design phase, and will require 4.5 to 5 gigajoules per pulse for its toroidal and poloidal coil systems. The understanding and control of charge and discharge processes under usual and abnormal conditions is essential for safe, reliable operation.

MIT has been carrying out a program for INEL oriented toward safety and protection in large-scale magnet systems. The program involves collection and analysis of information on actual magnet failures, analysis of general problems associated with safety and protection in systems of this type, and performance of safety-oriented experiments. This report summarizes work performed in FY86.

Last year, we reported [1] on the collaboration established with Kernforschungszentrum, Karlsruhe, FRG. Section 2.0 and 3.0 in this report describe analyses performed by our representative (M.M. Steeves) while on-site at KfK in support of their TESPE testing program.

In Section 2.0 currents and forces are calculated in support of the TESPE-S safety experiment of a six-coil arrangement with a single-coil lead-to-lead electrical short circuit. System current is the forcing function and current in the shorted coil is the electrical response. These currents are unequal on the average and therefore produce asymmetrical mechanical force distributions in TESPE. The current and force distributions are presented as functions of time.

The TESPE-S magnet-safety experiments are now focusing on simulation of a single toroidal coil failure due to a lead-to-lead electrical short circuit. The short circuit resistor has a design resistance of 1×10^{-6} ohms. This value is compatible with both the requirements of the safety program and with the cooling power available to the resistor. The lead-to-lead short creates an asymmetrical mechanical force distribution in TESPE. Dynamic centering forces on the shorted coil D1 and its 180° counterpart D4 are presented, as well as dynamic force distributions over the other four TESPE

[1] R.J. Thome, J.V. Minervini, R.D. Pillsbury, et al, "Safety and Protection for Large Scale Superconducting Magnets-FY85 Report", PFC/RR-85-25, Dec, 1985

coils. These forces are written in terms of influence coefficients and coil currents. Since the forces are given as functions of time, the mechanical response of TESPE can, in theory, be determined.

Section 3.0 presents analyses of a possible experiment in which a coil available at MIT (the "football" coil) could be used in a destructive experiment within TESPE. Results indicate that the coil is geometrically compatible with the facility and that burnout of the coil could probably be accomplished through joule heating resulting from inductive energy transfer between TESPE in a fast discharge and the test coil. However, the terminations on the "football" coil require completion, and power bus access at the site must be provided. Whether or not results can be expected to warrant the cost will be evaluated this year.

The fourth section presents the results of analyses performed following a problem detected in the testing of a coil constructed under a different program. In this case, a coil wound with an internally cooled cable superconductor (ICCS) developed several short circuits during construction. Coil performance was essentially unaffected when subjected to initial charge sequences, however, following a "dump" (fast discharge) the conductor was found to be unable to hold pressure. The analyses in Section 4.0 show that: 1) little damage would likely be done due to currents flowing through the shorts during a slow charge and 2) a "dump" from several hundred amperes could cause severe enough heating to damage the stainless steel sheath of the conductor.

Safety and protection analyses of subsystems becomes progressively more important as the stored energy increases with each step forward in the magnetic fusion program. The effort under this contract contributes to future safety and reliability by analyzing and understanding magnet operational problems as experienced in actual systems and test apparatus.

2 Short Circuit Calculations in Support of the TESPE Experiment

M.M. Steeves

2.1 Introduction

Currents and forces are calculated in support of the TESPE-S safety experiment of a six-coil arrangement with a single-coil lead-to-lead electrical short circuit. System current is the forcing function and current in the shorted coil is the electrical response. These currents are unequal on the average and therefore produce asymmetrical mechanical force distributions in TESPE. The current and force distributions are presented as functions of time.

The TESPE-S magnet-safety experiments are now focusing on a single toroidal coil failure due to a lead-to-lead electrical short circuit. The short circuit resistor has a design resistance of 1 x 10^{-6} ohms. This value is compatible with both the requirements of the safety program and with the cooling power available to the resistor. The lead-to-lead short creates an asymmetrical mechanical force distribution in TESPE. Dynamic centering forces on the shorted coil D1 and its 180° counterpart D4 are presented, as well as dynamic force distributions over the other four TESPE coils. These forces are written in terms of influence coefficients and coil currents. Since the forces are given as functions of time, the mechanical response of TESPE can, in theory, be determined.

L_1 = 44 mH (Coil D1)

L_5 = 266 mH

M = 11.6 mH

R_C = 340 + 240 B μΩ

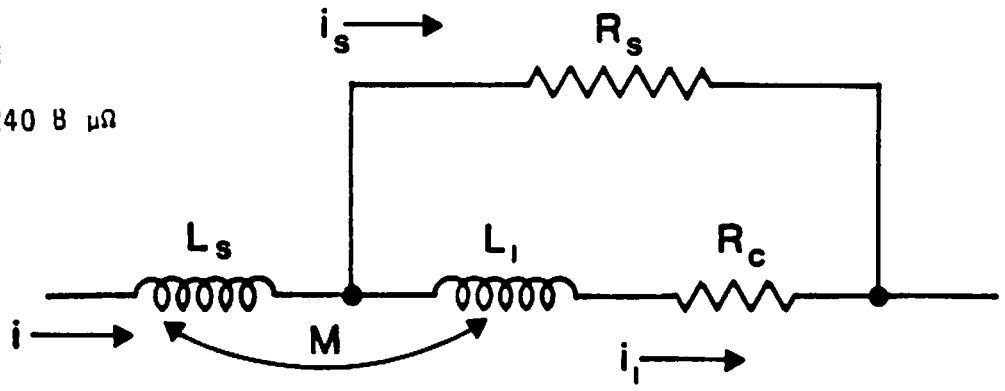

Figure 2.1 TESPE-S five-coil-experiment circuit model

2.2 Results

A summary of calculated results is given below.

2.2.1 Circuit Model

The TESPE-S circuit model, Figure 2.1, is that of two coupled inductors, one of which is shorted by a known resistor.

$$\tau_1 = \frac{L_1}{R_s + R_c}, \tau_m = \frac{M}{R_s + R_c}, r_s = \frac{R_s}{R_s + R_c} \tag{1}$$

2.2.2 Forcing Function

The system current i is the forcing function in this study. It is assumed to have the wave shapes shown in Figure 2.2.

2.2.3 System Response

Current through the shorted coil D1 is given below for the initial current ramp, for the flattop, and also for the discharge. Note that current through the resistive short is given by

$$i_s = i - i_1 \tag{2}$$

$\underline{t < t_1}$

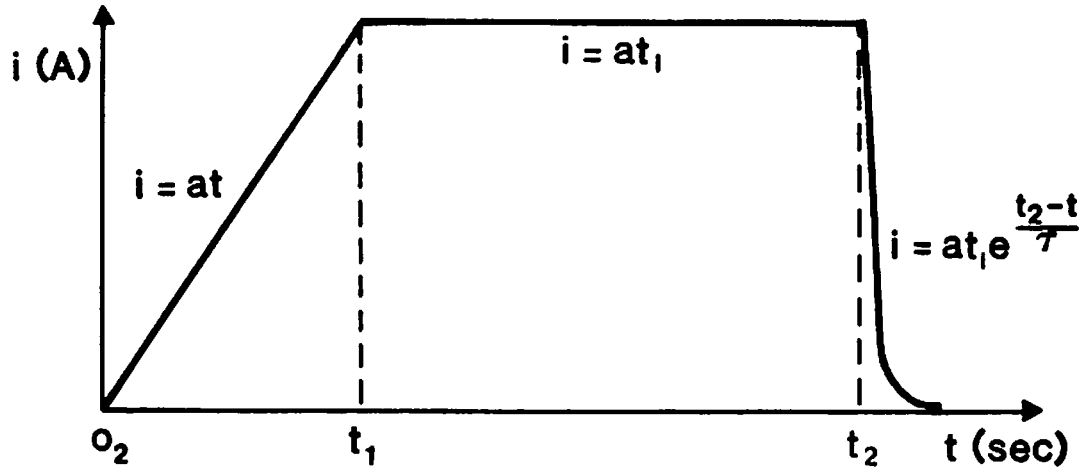

Figure 2.2 Assumed waveshape of the system circuit

$$i_1 = a(\tau_1 r_s + \tau_m)(e^{\frac{-t}{\tau_1}} - 1) + a r_s t \tag{3}$$

$\underline{t_1 \leq t \leq t_2}$

$$i_1 = a(\tau_1 r_s + \tau_m)(e^{\frac{-t}{\tau_1}} - e^{\frac{t_1 - t}{\tau_1}}) + a r_s t_1 \tag{4}$$

$\underline{t > t_2}$

If $\tau \neq \tau_1$,

$$i_1 = i_{1,2} e^{\frac{t_2 - t}{\tau_1}} + a t_1 \left[\frac{\tau r_s + \tau_m}{\tau - \tau_1}\right]\left[e^{\frac{t_2 - t}{\tau}} - e^{\frac{t_2 - t}{\tau_1}}\right] \tag{5}$$

If $\tau = \tau_1$,

$$i = \left[a t_1 (\frac{\tau_1 r_s + \tau_m}{\tau_1})(\frac{t - t_2}{\tau_1}) + i_{1,2}\right] e^{\frac{t_2 - t}{\tau_1}} \tag{6}$$

where $i_{1,2} = i_1(t = t_2)$ in Eq. (4). Figure 2.3 is a sketch of a *typical* response when$R_c = 0$.

2.2.4 Maximum Negative Current

When the current in TESPE is ramped, current in the shorted coil (see Figure 2.4) reaches a negative maximum if the ramp duration is long.

$$t_m = -\tau_1 ln \left[\frac{r_s}{r_s + \tau_m/\tau_1}\right] \tag{7}$$

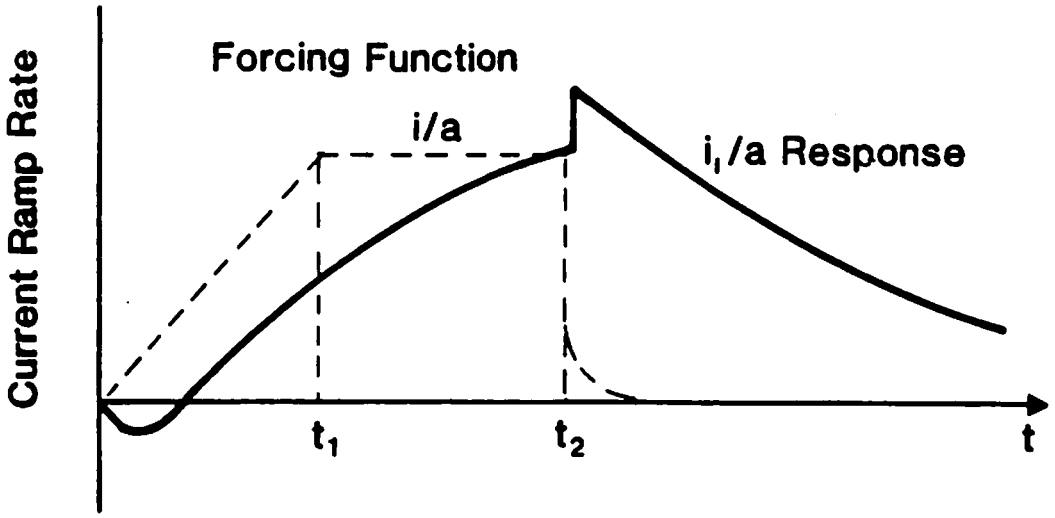

Figure 2.3 Sketch of a *typical* response when $R_c = 0$

$$i_{1m} = -a\left[\tau_m + \tau_1 ln(\frac{\tau_1}{\tau_m})\right] \tag{8}$$

For $R_c = 0$ only,

$$t_0 = \frac{21.945 \times 10^{-3}}{R_s} \tag{9}$$

2.2.5 Net Radial Force on Shorted Coil D1

The net radially directed force on coil D1 can be written as the product of its current, the system current, and a constant. The constant is geometry dependent and has been calculated using the computer program EFFI. It can be called an influence coefficient and has the numerical value of

$$k = -2.56 \times 10^{-2} \frac{N}{A^2} \tag{10}$$

Thus, the radial force(x-directed in the EFFI global coordinate system) on coil D1 as a function of time reads $F = kii_1$:

$\underline{t < t_1}$

$$F_r = ka^2 t\left[(\tau_1 r_s + \tau_m)(e^{\frac{-t}{\tau_1}} - 1) + r_s t\right] \tag{11}$$

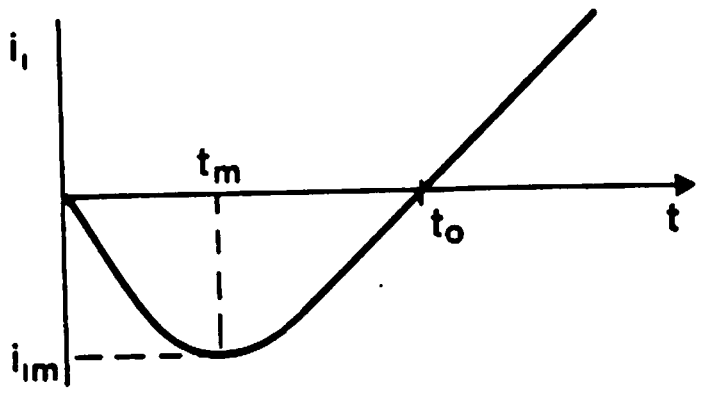

Figure 2.4 Current in shorted coil

$\underline{t_1 \leq t \leq t_2}$

$$F_r = ka^2 t_1 \left[(\tau_1 r_s + \tau_m)(e^{\frac{-t}{\tau_1}} - e^{\frac{t_1 - t}{\tau_1}}) + r_s t_1 \right] \tag{12}$$

$\underline{t_2 > t}$
$\tau \neq \tau_1$:

$$F_r = ka^2 t_1 e^{\frac{t_2 - t}{\tau}} \left[\frac{i_{1,2}}{a} e^{\frac{t_2 - t}{\tau_1}} + t_1 (\frac{\tau r_s + \tau_m}{\tau - \tau_1})(e^{\frac{t_2 - t}{\tau}} - e^{\frac{t_2 - t}{\tau_1}} \right] \tag{13}$$

$\tau = \tau_1$:

$$F_r = ka^2 t_1 e^{\frac{2(t_2 - t)}{\tau_1}} \left[\frac{i_{1,2}}{a} + t_1 (\frac{\tau_1 r_s + \tau_m}{\tau_1})(\frac{t - t_2}{\tau_1}) \right] \tag{14}$$

where $i_{1,2} = i_1(t = t_2)$ in Eq. (4). Note that a positive radial force (in the positive x - direction) tends to move coil D1 away from the TESPE vertical centerline, and therefore represents a serious and potentially disastrous structural load.

2.2.6 Maximum Radially Outward Force

If the current ramp duration is comparable to the time constant of the shorted coil, then the radially outward force maximizes at a time given by the solution of the equation.

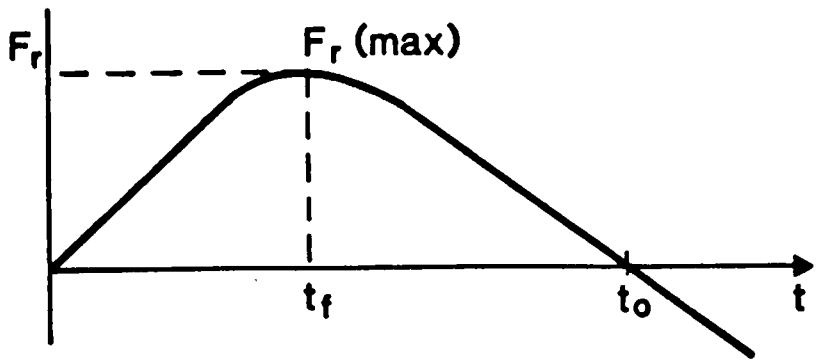

Figure 2.5 Radial force on shorted coil as a function of time

$$e^{\frac{-t_f}{\tau_1}}\left(1-\frac{t_f}{\tau_1}\right)+\left(\frac{2r_s}{\tau_1 r_s+\tau_m}\right)t_f-1=0 \tag{15}$$

where t_f is defined in Fig. 2.5.

For $R_c = 0$ only,

$$t_f=\frac{14.05\times 10^{-3}}{R_s} \tag{16}$$

$$F_r(max)=ka^2t_f\left[(\tau_1 r_s+\tau_m)(e^{\frac{-t_f}{\tau_1}}-1)+r_s t_f\right] \tag{17}$$

Figure 2.6 shows radial force normalized to the square of current ramp rate plotted against time when coil D1 is shorted by a 1 $\mu\Omega$ resistor. In this case $t_f = 14.05 \times 10^3$ seconds.

2.2.7 Influence Coefficients for Coils D2 – D3

The TESPE D-coils have been modeled for purposes of force calculations as connections of current-carrying elements in the computer program EFFI. The x and y components of force on the centroid of any element can be written in terms of influence coefficients. In this way, the influence of a different current in coil D1 on the entire TESPE coil system can be studied. The x-component of force on the centroid of element p-q (called current segment p-q) is influenced by the current i in coils D2- D6 and by the current i_1 in coil D1. When segment p-q lies in either coil D2 or D3, the x-component of force on the centroid of p-q reads

$$F_{x,p-q}^{i,i_1} = G_{x,p-q}^{2-6} i^2 + G_{x,p-q}^{1} i i_1 \tag{18}$$

where $G_{x,p-q}^{2-6}$ = x - directed influence coefficient for segment p-q due to current i in coils D2-D6, and $G_{x,p-q}^{1}$ = x-directed influence coefficient for segment p-q due to current i_1 in coil D1 and i in D2 – D6.

An expression similar to Eq. (18) holds for the y-component of force. When current in coil D1 equals the system current, Eq.(18) reduces to

$$F_{x,p-q}^{i,i} = G_{x,p-q}^{1-6} i^2 \tag{19}$$

where

$$G_{x,p-q}^{1-6} = G_{x,p-q}^{1} + G_{x,p-q}^{2-6} \tag{20}$$

The influence coefficients allow one to find the force distributions as functions of time. Knowledge of TESPE mechanical stiffnesses should yield mechanical deflections as the system response. Figure 2.7 shows how EFFI can be used to approximate the middle curve of the TESPE D-coil by straight lines that connect the end-plane centroids of what are called general current elements (GCEs). The centroids of the GCEs are marked by crosses. These are the points at which segment force components are given. Force components in terms of influence coefficients are summarized in tables 2.1 and 2.2. The global coordinate system for TESPE is shown in Figure 2.8.

Table 2.1 TESPE coil D2 x and y force components on current segment centroids. Current in coil D1 is denoted by i_1. System current is denoted by i. Forces are in Newtons.

X- Components of Force (N)

$F_{x,1-1}^{ii_1} = 2.90\times10^{-3}\, i^2 + 9.28\times10^{-4}\, ii_1$	$F_{x,1-1}^{ii} = -3.83\times10^{-3}\, i^2$
$F_{x,1-2}^{ii_1} = 2.45\times10^{-3}\, i^2 + 9.28\times10^{-4}\, ii_1$	$F_{x,1-2}^{ii} = 3.38\times10^{-3}\, i^2$
$F_{x,1-3}^{ii_1} = 1.58\times10^{-3}\, i^2 + 8.29\times10^{-4}\, ii_1$	$F_{x,1-3}^{ii} = 2.47\times10^{-3}\, i^2$
$F_{x,2-1}^{ii_1} = 2.59\times10^{-4}\, i^2 + 6.75\times10^{-4}\, ii_1$	$F_{x,2-1}^{ii} = 9.34\times10^{-3}\, i^2$
$F_{x,2-2}^{ii_1} = -9.41\times10^{-4}\, i^2 + 6.18\times10^{-4}\, ii_1$	$F_{x,2-2}^{ii} = -3.23\times10^{-4}\, i^2$
$F_{x,3-1}^{ii_1} = -3.14\times10^{-3}\, i^2 + 6.18\times10^{-4}\, ii_1$	$F_{x,3-1}^{ii} = -2.52\times10^{-3}\, i^2$
$F_{x,4-1}^{ii_1} = -3.16\times10^{-3}\, i^2 + 2.32\times10^{-4}\, ii_1$	$F_{x,4-1}^{ii} = -3.93\times10^{-3}\, i^2$
$F_{x,4-2}^{ii_1} = -3.82\times10^{-3}\, i^2 + 7.73\times10^{-5}\, ii_1$	$F_{x,4-2}^{ii} = -3.74\times10^{-3}\, i^2$
$F_{x,5-1}^{ii_1} = -7.08\times10^{-3}\, i^2 - 2.32\times10^{-4}\, ii_1$	$F_{x,5-1}^{ii} = -7.37\times10^{-3}\, i^2$
$F_{x,Net}^{ii_1} = -2.20\times10^{-2}\, i^2 + 9.58\times10^{-3}\, ii_1$	$F_{x,Net}^{ii} = -1.24\times10^{-2}\, i^2$

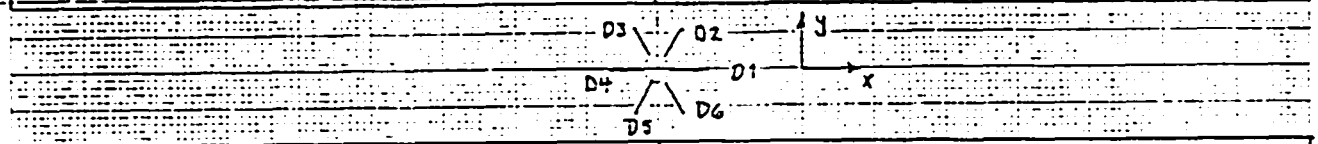

Y- Components of Force (N)

$F_{y,1-1}^{ii_1} = 6.39\times10^{-3}\, i^2 + 1.55\times10^{-4}\, ii_1$	$F_{y,1-1}^{ii} = 6.54\times10^{-3}\, i^2$
$F_{y,1-2}^{ii_1} = 5.65\times10^{-3}\, i^2 + 7.73\times10^{-5}\, ii_1$	$F_{y,1-2}^{ii} = 5.73\times10^{-3}\, i^2$
$F_{y,1-3}^{ii_1} = 4.27\times10^{-3}\, i^2$	$F_{y,1-3}^{ii} = 4.27\times10^{-3}\, i^2$
$F_{y,2-1}^{ii_1} = 1.80\times10^{-3}\, i^2 - 1.70\times10^{-4}\, ii_1$	$F_{y,2-1}^{ii} = 1.63\times10^{-3}\, i^2$
$F_{y,2-2}^{ii_1} = -7.11\times10^{-4}\, i^2 - 4.49\times10^{-4}\, ii_1$	$F_{y,2-2}^{ii} = -5.60\times10^{-4}\, i^2$
$F_{y,3-1}^{ii_1} = -3.22\times10^{-3}\, i^2 - 1.16\times10^{-3}\, ii_1$	$F_{y,3-1}^{ii} = -4.38\times10^{-3}\, i^2$
$F_{y,4-1}^{ii_1} = -3.82\times10^{-3}\, i^2 - 1.24\times10^{-3}\, ii_1$	$F_{y,4-1}^{ii} = -5.06\times10^{-3}\, i^2$
$F_{y,4-2}^{ii_1} = -4.82\times10^{-3}\, i^2 - 1.70\times10^{-3}\, ii_1$	$F_{y,4-2}^{ii} = -6.52\times10^{-3}\, i^2$
$F_{y,5-1}^{ii_1} = -9.16\times10^{-3}\, i^2 - 3.48\times10^{-7}\, ii_1$	$F_{y,5-1}^{ii} = -1.26\times10^{-2}\, i^2$
$F_{y,Net}^{ii_1} = -6.04\times10^{-3}\, i^2 - 1.59\times10^{-2}\, ii_1$	$F_{y,Net}^{ii} = -2.20\times10^{-2}\, i^2$

Example: System current $i = 7000$ A and D1 current $i_1 = 2770$ A

coil D2 Segment 2-1: $F_{x,2-1}^{ii_1} = 2.59\times10^{-4}(7000)^2 + 6.75\times10^{-4}(7000)(2770) = 2.29\times10^{4}$ N

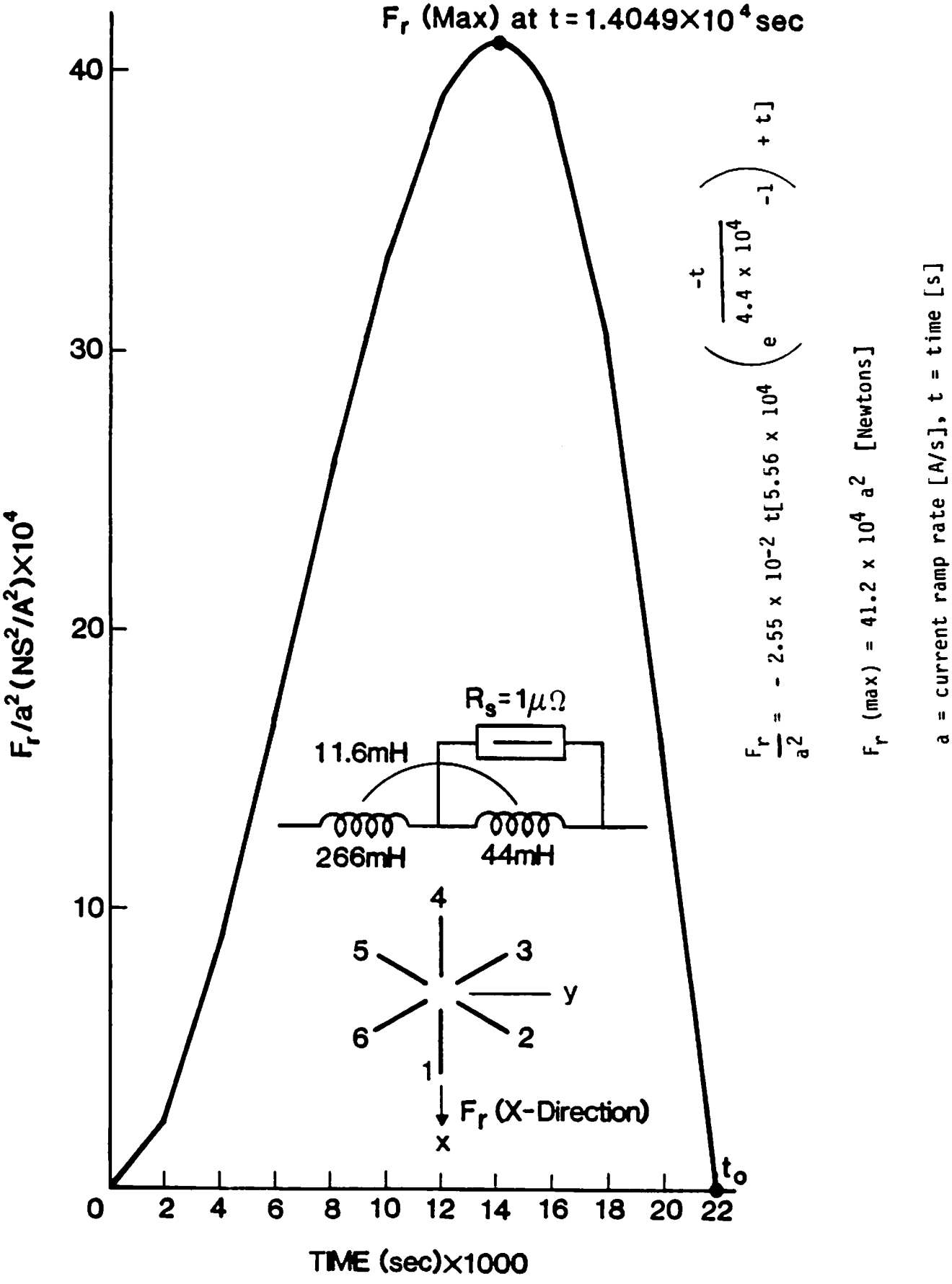

Figure 2.6 TESPE coil-D1 radial force normalized to current ramp rate as a function of time. Positive force has a radially outward direction. As an example, if ramp rate a = 0.01 A/s, the F_r(max) = 41.2 N

Seg. p-q	Centroid Coordinates R(mm)	T(mm)
1-1	919	71
1-2	868	202
1-3	772	306
2-1	660	362
2-2	548	373
3-1	429	338
4-1	345	265
4-2	307	189
5-1	293	73

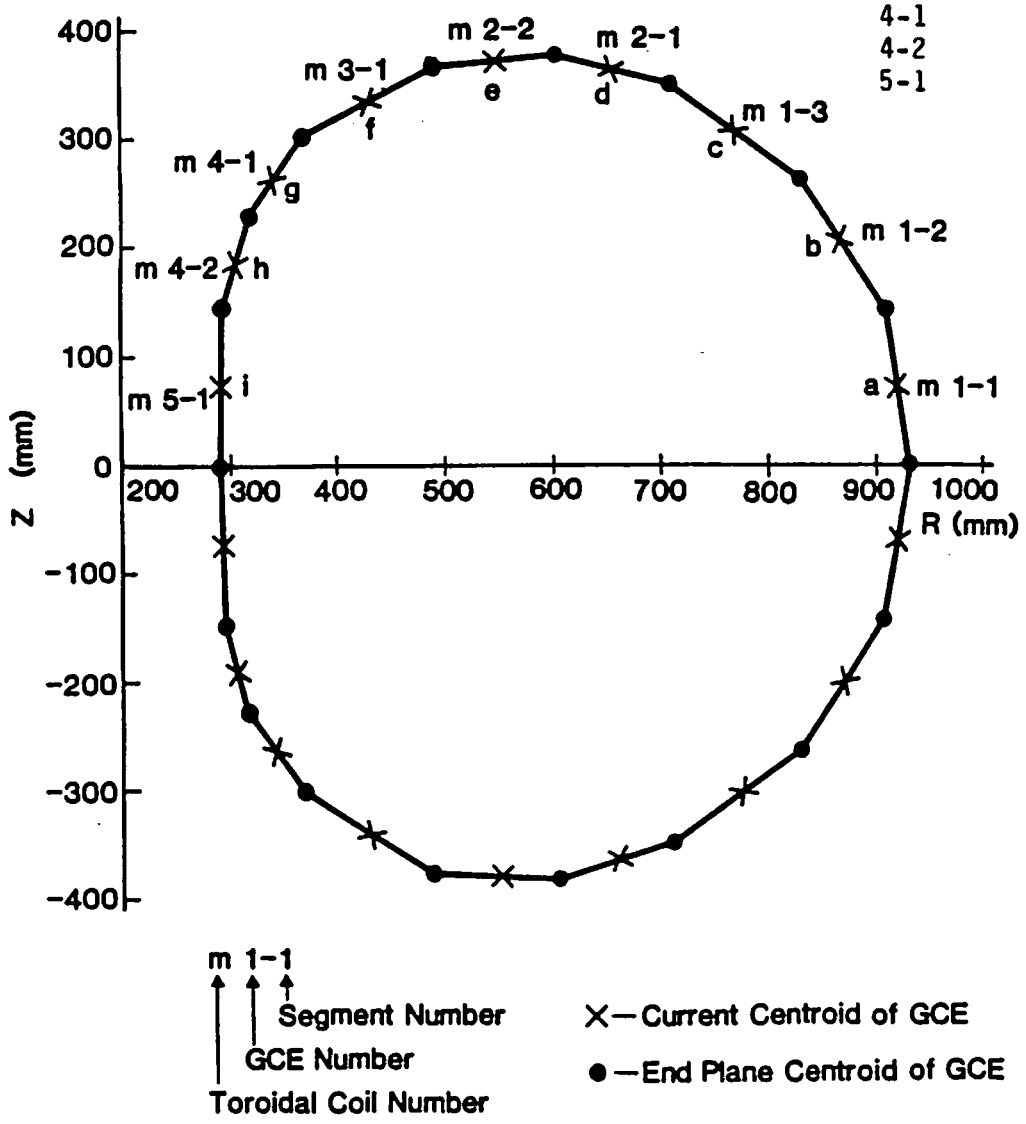

Figure 2.7 Straight-line approximation of TESPE D-coil middle curve generated by the program EFFI. The end-plane centroids of general current elements are connected by solid circles. The crosses locate GCE centroids and are the points where force components are given

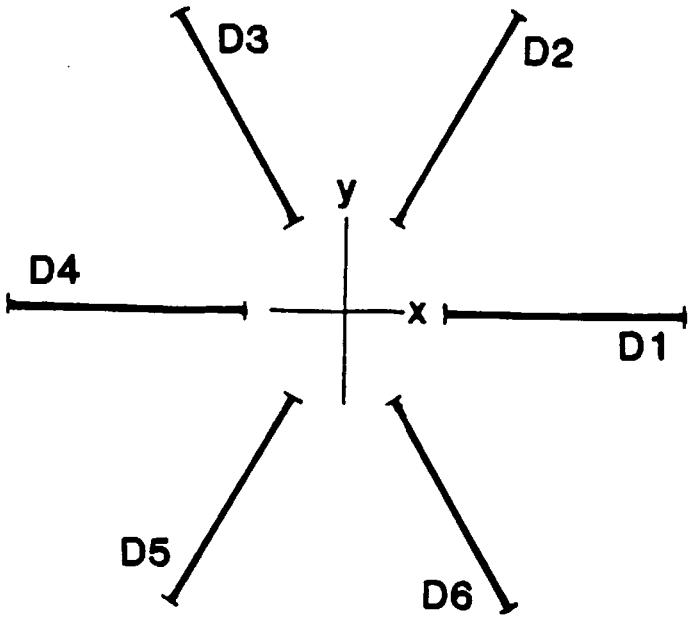

Figure 2.8 TESPE global coordinate system used for EFFI calculations. Note that coil D1 lies on the positive x-axis.

Table 2.2 TESPE coil D3 x and y force components on current segment centroids. Current in coil D1 is denoted by i_1. System current is denoted by i. Forces are in Newtons.

X-Components of Force (N)

$F_{x,1-1}^{i i_1} = -3.82\times10^{-3}\, i^2$	$F_{x,1-1}^{i\,i} = -3.82\times10^{-3}\, i^2$
$F_{x,1-2}^{i i_1} = -3.37\times10^{-3}\, i^2 + 7.73\times10^{-5}\, i i_1$	$F_{x,1-2}^{i\,i} = -3.29\times10^{-3}\, i^2$
$F_{x,1-3}^{i i_1} = -2.51\times10^{-3}\, i^2 + 7.73\times10^{-5}\, i i_1$	$F_{x,1-3}^{i\,i} = -2.43\times10^{-3}\, i^2$
$F_{x,2-1}^{i i_1} = -1.00\times10^{-3}\, i^2 + 5.41\times10^{-5}\, i i_1$	$F_{x,2-1}^{i\,i} = -9.46\times10^{-4}\, i^2$
$F_{x,2-2}^{i i_1} = 2.29\times10^{-4}\, i^2 + 9.82\times10^{-5}\, i i_1$	$F_{x,2-2}^{i\,i} = 3.27\times10^{-4}\, i^2$
$F_{x,3-1}^{i i_1} = 2.37\times10^{-3}\, i^2 + 2.32\times10^{-4}\, i i_1$	$F_{x,3-1}^{i\,i} = 2.60\times10^{-3}\, i^2$
$F_{x,4-1}^{i i_1} = 2.76\times10^{-3}\, i^2 + 1.55\times10^{-4}\, i i_1$	$F_{x,4-1}^{i\,i} = 2.92\times10^{-3}\, i^2$
$F_{x,4-2}^{i i_1} = 3.53\times10^{-3}\, i^2 + 2.32\times10^{-4}\, i i_1$	$F_{x,4-2}^{i\,i} = 3.76\times10^{-3}\, i^2$
$F_{x,5-1}^{i i_1} = 6.84\times10^{-3}\, i^2 + 4.64\times10^{-4}\, i i_1$	$F_{x,5-1}^{i\,i} = 7.30\times10^{-3}\, i^2$
$F_{x,Net}^{i i_1} = 1.00\times10^{-2}\, i^2 + 2.78\times10^{-3}\, i i_1$	$F_{x,Net}^{i\,i} = 1.28\times10^{-2}\, i^2$

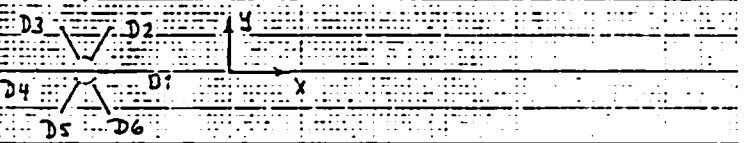

Y-Components of Force (N)

$F_{y,1-1}^{i i_1} = 6.37\times10^{-3}\, i^2 + 1.55\times10^{-4}\, i i_1$	$F_{y,1-1}^{i\,i} = 6.53\times10^{-3}\, i^2$
$F_{y,1-2}^{i i_1} = 5.59\times10^{-3}\, i^2 + 1.55\times10^{-4}\, i i_1$	$F_{y,1-2}^{i\,i} = 5.75\times10^{-3}\, i^2$
$F_{y,1-3}^{i i_1} = 4.10\times10^{-3}\, i^2 + 1.55\times10^{-4}\, i i_1$	$F_{y,1-3}^{i\,i} = 4.26\times10^{-3}\, i^2$
$F_{y,2-1}^{i i_1} = 1.53\times10^{-3}\, i^2 + 9.28\times10^{-5}\, i i_1$	$F_{y,2-1}^{i\,i} = 1.62\times10^{-3}\, i^2$
$F_{y,2-2}^{i i_1} = -5.90\times10^{-4}\, i^2 + 3.09\times10^{-5}\, i i_1$	$F_{y,2-2}^{i\,i} = -5.59\times10^{-4}\, i^2$
$F_{y,3-1}^{i i_1} = -4.31\times10^{-3}\, i^2 - 7.73\times10^{-5}\, i i_1$	$F_{y,3-1}^{i\,i} = -4.39\times10^{-3}\, i^2$
$F_{y,4-1}^{i i_1} = -4.90\times10^{-3}\, i^2 - 2.32\times10^{-4}\, i i_1$	$F_{y,4-1}^{i\,i} = -5.13\times10^{-3}\, i^2$
$F_{y,4-2}^{i i_1} = -6.20\times10^{-3}\, i^2 - 3.87\times10^{-4}\, i i_1$	$F_{y,4-2}^{i\,i} = -6.59\times10^{-3}\, i^2$
$F_{y,5-1}^{i i_1} = -1.19\times10^{-2}\, i^2 - 7.73\times10^{-4}\, i i_1$	$F_{y,5-1}^{i\,i} = -1.27\times10^{-2}\, i^2$
$F_{y,Net}^{i i_1} = -2.06\times10^{-2}\, i^2 - 1.76\times10^{-3}\, i i_1$	$F_{y,Net}^{i\,i} = -2.24\times10^{-2}\, i^2$

Example: System current $i = 7000$ A and D1 current $i_1 = 2170$ A

Coil D3 Segment 4-2: $F_{y,4-2}^{i i_1} = -6.20\times10^{-3}(7000)^2 - 3.87\times10^{-4}(7000)(2170) = -3.10\times10^{5}$ N

2.2.8 Net Radial Force on Coil D4

The net radial force on TESPE coil D4 can be written in terms of influence coefficients as

$$F_{x,net}^{i,i_1} = 2.38 \times 10^{-2} i^2 + 1.00 \times 10^{-3} i, i_1 \tag{21}$$

where i = system current (D2 - D6), and i_1 = coil D1 current.

When i_1 = i, this reduces to

$$F_{x,net}^{i,i} = 2.48 \times 10^{-2} i^2 \tag{22}$$

2.2.9 Shorting Resistor Power

Power dissipated in the short circuit resistor is given below.

$\underline{t < t_1}$

$$P_s = \left[t(1 - r_s) - (\tau_1 r_s - \tau_m)(\epsilon^{\frac{-t}{\tau_1}} - 1) \right]^2 a^2 R_s \tag{23}$$

$\underline{t_1 \leq t \leq t_2}$

$$P_s = \left[t_1(1 - r_s) - (\tau_1 r_s + \tau_m)(\epsilon^{\frac{-t}{\tau_1}} - e^{\frac{t_1 - t}{\tau_1}}) \right]^2 a^2 R_s \tag{24}$$

$\underline{t > t_2}$

$\tau \neq \tau_1$:

$$P_s = \left[t_1 e^{\frac{t_2 - t}{\tau}} - \frac{i_{c2}}{a} e^{\frac{t_2 - t}{\tau_1}} - t_1 \left(\frac{\tau r_s + \tau_m}{\tau - \tau_1} \right) (\epsilon^{\frac{t_2 - t}{\tau}} - e^{\frac{t_2 - t}{\tau_1}}) \right]^2 a^2 R_s \tag{25}$$

$\tau = \tau_1$:

$$P_s = \left[t_1 e^{\frac{t_2 - t}{\tau}} - \left(\frac{i_{c2}}{a} + t_1 \left(\frac{\tau_1 r_s + \tau_m}{\tau_1} \right) \left(\frac{t - t_2}{\tau_1} \right) \right) e^{\frac{t_2 - t}{\tau_1}} \right]^2 a^2 R_s \tag{26}$$

2.2.10 Current Jump in D1 Due to System Discharge

If $i_1(t_2)$ is the initial current in coil D1 prior to a discharge of TESPE, then immediately after discharge, the current in D1 will rise to a value given by

$$i_1(t_2^+) = \left(\frac{L_1 + M}{L_1} \right) i_1(t_2) = 1.26 i_1(t_2) \tag{27}$$

2.2.11 Upper Bound on D1 Coil Current Due to Resistor Power

The maximum power in the shorting resistor R_s is limited to approximately 49 watts. Since current in coil D1 will jump by 26% when TESPE current is discharged through an external resistor, there exists an upper bound on D1 current prior to discharge of TESPE. This maximum allowable current due to resistor heating is approximately

$$max.i_1(t_2) \approx \frac{7000A}{1.26} = 5556A. \tag{28}$$

2.3 Nomenclature for Section 2

Symbol	Definition	Units
a	TESPE system current rate of rise (ramp rate)	A/S
B	Magnetic field at coil D1	T
F_R	Net radial force on coil D1	N
$F^{i,i_1}_{x,p-q}$	X and Y components of force on the centroid of current segment p-q when system current is i and coil D1 current is i_1. See EFFI.	N
$F^{i,i_1}_{y,p-q}$		
$G^{2-6}_{x,p-q}$	X and Y influence coefficients for the centroid of current segment p-q due to system current i in coils D2-D6. Segment p-q lies in either D2 or D3.	N/A^2
$G^{2-6}_{y,p-q}$		
$G^{1}_{x,p-q}$	X and Y influence coefficients for the centroid of current segment p-q due to system current i in coils D2-D6 and current i_1 in D1. Segment p-q lies in either D2 or D3.	N/A^2
$G^{1}_{y,p-q}$		
$G^{1-6}_{x,p-q}$	X and Y influence coefficients when all coils carry system current i. Segment p-q lies in either D2 or D3.	N/A^2
$G^{1-6}_{y,p-q}$		
i	System current (from power supply)	A
i_1	Current in TESPE coil D1	A
i_s	Current in short circuit resistor	A
i_{1m}	Peak negative current in shorted coil D1	A
$i_{1,2}$	Current in coil D1 at time t_2 (beginning of system dump)	A
$i_1(t_2^+)$	Current in coil D1 at time $t_2 + \Delta t$, where Δt is small (shortly after the beginning of system dump)	A
k	Influence coefficient for TESPE coil D1. The radial force on D1 (x - direction in global EFFI coordinates) is defined to be $F_r = k\ i i_1$	N/A^2

Symbol	Definition	Units
L_1	Self inductance of TESPE coil D1	H
L_5	Self inductance of TESPE coils D2-D4 together	H
M	Mutual inductance between D1 and D2-D4	H
P_s	Power dissipated in the short circuit resistor R_S	W
R_c	Normal resistance of coil D1	Ω
R_s	Short-circuit resistance	Ω
r_s	Resistance ratio defined in Eq. (1)	
t	Time	s
t_1	Time at end of system current ramp	s
t_2	Time at end of system current flattop	s
t_m	Time at which current in coil D1 reaches a negative maximum. See Eq. (7)	s
t_o	Time at which current in coil D1 passes through zero. See Eq. (9)	s
t_f	Time at which the net radial force on coil D1 reaches a positive maximum (positive direction is radially outward away from the TESPE vertical centerline)	s
τ	Time constant of TESPE system current discharge into an external dump resistor	s
τ_1	Time constant of shorted coil D1. See Eq. (1)	s
τ_m	Time constant from mutual inductance between D1 and D2-D6 and D1 resistance. See Eq. (1)	s

3 PRELIMINARY EVALUATION OF THE "FOOTBALL" COIL FOR USE IN A TESPE EXPERIMENT

M.M. Steeves

3.1 Introduction

Calculations supporting a proposed destructive experiment of a superconducting test coil ("Football") are given. The test coil could be inductively heated by the discharge of TESPE. The resulting temperature rise as a function of TESPE current and discharge time constant are estimated.

The test coil, called Module 4 ("Football"), was wound in a racetrack geometry by MIT in 1980 and is nearly finished, needing only current terminations on its leads. It consists of a 20-meter length of cable-in-conduit (ICCS) conductor with a NbTi superconductor, which has a critical current of approximately 30,000 amperes at 6 T and 4.2 K.

The analysis as sumes that Module 4 has shorted leads. When TESPE discharges, it induc- tively heats Module 4 with the temperature rise depending on the current in TESPE and the discharge time constant.

3.2 Assumptions

The following assumptions were made in the estimation of the Module 4 (football coil) temperature rise.

1. The geometric center of the Module 4 coil is at a radius of R = 600 mm and an elevation of Z = 0 mm above the TESPE D-coil midplane.
2. The middle curve of the Module 4 coil can be used to estimate its self and mutual inductances.
3. Magnetic field in TESPE is a function of radius only.
4. Critical current of the NbTi ICCS conductor is 25,000 A at 7 T.
5. Temperature rise can be calculated assuming the entire 20 m length of the Module 4 coil is normal (not superconducting).

6. Magnetoresistance at B = 3.5 T is reasonable.
7. The integral $\int_{4k}^{T} \frac{\gamma C_p}{\rho} dT$ can be approximated by $Z_0\sqrt{\frac{T}{T_0}}$.
8. The induced current in Module 4 at time t = 0 seconds is zero.
9. At T_0 = 200 K, Z_0= 10^{17} $A^2 \cdot s \cdot m^{-4}$.
10. Module 4 is electrically shorted across its terminals by a 1 $\mu\Omega$ resistor.
11. The specific heats of the NbTi, helium, and stainless steel conduit can be neglected. That is, temperature rise is calculated assuming Module 4 to be a copper cable.
12. The resistance R_2 of Module 4 is independent of temperature.
13. The TESPE magnetic field is purely azimuthal.
14. Heating of Module 4 is adiabatic with no heat transfer to the surroundings.

3.3 Results

3.3.1 Temperature Rise

The temperature rise of the Module 4 (football) coil as a function of TESPE operating current and decay time constant is

$$T = \frac{T_0}{Z_0^2}\left(\frac{Mi_0}{\sqrt{2}A_{cu}R_2}\right)^4 \frac{1}{(\tau + \tau_2)^2} \tag{29}$$

where

Symbol	Definition	Unit
T	Temperature rise of the ICCS above 4 K	K
T_0	Temperature at curve fit $Z = Z_0\sqrt{\frac{T}{T_0}}$	K
Z_0	$\int_{4k}^{T_0} \frac{\gamma C_p}{\rho} dt$	$A^2 \cdot s \cdot m^{-4}$
γ	Mass density of copper	$kg \cdot m^{-3}$
C_p	Specific heat of copper	$J \cdot kg^{-1} \cdot K^{-1}$
ρ	Electrical resistivity of copper	$\Omega \cdot m$
M	Mutual inductance between Module 4 and TESPE	H
i_0	Peak current in TESPE	A
A_{cu}	ICCS cable copper cross-sectional area	m^2
R_2	Resistance of Module 4, including short across coil terminals	Ω
τ	Discharge time constant of TESPE	s
τ_2	$\frac{L_2}{R_2}$	s
L_2	Self inductance of Module 4	H

Figure 3.1 shows T as a function of i_0 with τ as a parameter. It shows, for example, that the cable copper will melt if TESPE is discharged from 5,400 A with a 3 second time constant. This figure assumes that the initial current in the Module 4 coil is zero amperes.

3.3.2 Induced Current When $\tau \neq \tau_2$

When the TESPE discharge time constant does not equal the Module 4 time constant, the induced current as a function of time reads

$$i_2 = \frac{Mi_0}{R_2(\tau - \tau_2)}(e^{\frac{-t}{\tau}} - e^{\frac{-t}{\tau_2}}) + i_2(0)e^{\frac{-t}{\tau_2}} \tag{30}$$

where $i_2(0) = i_2$ (t = 0).

3.3.3 Induced Current When $\tau = \tau_2$

In this case the induced current as a function of time reads

$$i_2 = \frac{Mi_0}{L_2\tau_2} te^{\frac{-t}{\tau_2}} + i_2(0)e^{\frac{-t}{\tau_2}} \tag{31}$$

Figure 3.2 illustrates the behavior of i_2 as a function of time. The time constant $\tau_2 = L_2/R_2$ decreases by approximately two orders of magnitude when i_2 reaches the critical current of NbTi superconductor.

3.3.4 Estimated Coil Parameters

Parameters associated with the calculation of Module 4 temperature rise are listed below.

$M = 1.5$ mH $\quad A_{cu} = 89$ mm^2

$L_2 = 70\ \mu$H $\qquad R_2 = 63\ \mu\Omega$

$\tau_2 \approx 1$ s

Note that the resistance R_2 has two components: joint resistance and cable resistance.

$$R_2 = R_j + R_c \tag{32}$$

Joint resistance has been estimated to be perhaps $R_j = 1\ \mu\Omega$. Cable resistance at B = 0 T and RRR = 100, reads

$$R_c = \frac{\rho l}{A_{cu}} = \frac{(1.55 \times 10^{-10}\Omega \cdot m)(20m)}{89 \times 10^{-6}m^2} = 35\mu\Omega$$

at $B \neq 0$ T

$$R_c \approx 35\mu\Omega(1 + 0.22B) \tag{33}$$

and at B = 3.5 T

$$R_c \approx 35\mu\Omega(1 + 0.22(3.5)) = 62\mu\Omega \tag{34}$$

3.4 Analysis

3.4.1 Estimate of Module 4 Coil Inductances

The mutual inductance between the TESPE torus and the Module 4 racetrack can be calculated by writing the flux linkage of the middle curve of the Module 4 coil due to current in TESPE.

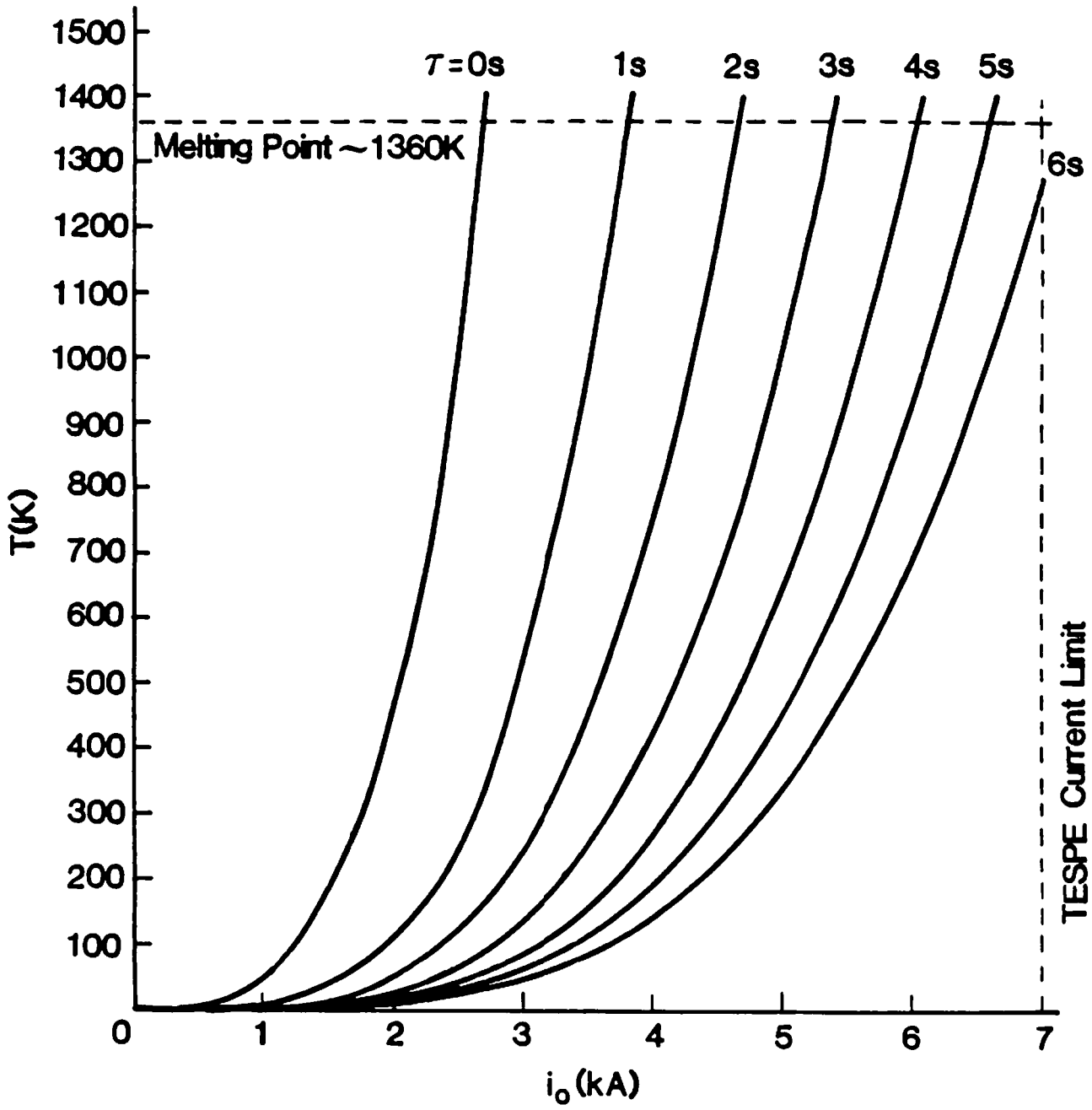

$$T = \frac{T_0}{L_0^2} \left(\frac{m\, i_o}{\sqrt{2}\, A_{cu}\, R_2} \right)^4 \frac{1}{(\tau + \tau_2)^2}$$

$$T = 2.561 \times 10^{-11} \frac{i_o^4}{(\tau + 1)^2}$$

$T_0 = 200$ K $Z_0 = 10^{17} \frac{A^2 \cdot s}{m^4}$

$M = 1.5$ mH $A_{cu} = 89 \times 10^{-6}$ m^2

$L_2 = 70$ μH $R_2 = 63$ μΩ

$\tau_2 = \frac{L_2}{R_2} = 1$ sec

Figure 3.1 Module 4 (football) coil temperature as a function of maximum TESPE current, i_0 and time discharge constant τ. It is assumed that the initial induced current in the module 4 coil is zero amperes and that R_2 is constant.

$$M = \frac{N_t \phi}{i} = 2N_t \int_{R_i}^{R_0} \frac{\mu_0 N}{2\pi R} h dR \tag{35}$$

where

Symbol	Definition
N_t	Number of turns in Module 4 (9 turns)
i	Current in TESPE [A]
Φ	Flux linking the middle curve of Module 4 [webers]
μ_0	$4\pi \times 10^{-7}[H \cdot m^{-1}]$
N	Number of turns in TESPE (1440 turns)
R	Radius measured from TESPE vertical centerline
h	Height of Module 4 middle curve at some R [m]

Equation (35) can be approximated by

$$M = \frac{N_t N \mu_0}{\pi} \sum_{i=1}^{n} \frac{h_i \Delta R_i}{R_i} \tag{36}$$

where for n = 8 (see Fig. 3.3)

$$\sum_{i=1}^{8} \frac{h_i \Delta R_i}{R_i} \cong 0.294m \tag{37}$$

Thus

$$M = \frac{9(1440)(4\pi \times 10^{-7})(0.294)}{\pi} = 1.5mH$$

with an uncertainty of perhaps ±0.5 mH.

The self inductance may be estimated from a formula for solenoids. The equivalent diameter of the middle curve is

$$d = \sqrt{\frac{4A_4}{\pi}} = \sqrt{\frac{4(434.429 + \pi(217)^2)}{\pi}} = 652mm$$

where A_4 = area enclosed by the middle curve of Module 4.

With reference to Fig. 3.4, the self inductance of the Module 4 coil reads

$$L_2 = r_i N_t^2 \theta(\alpha, \beta) \tag{38}$$

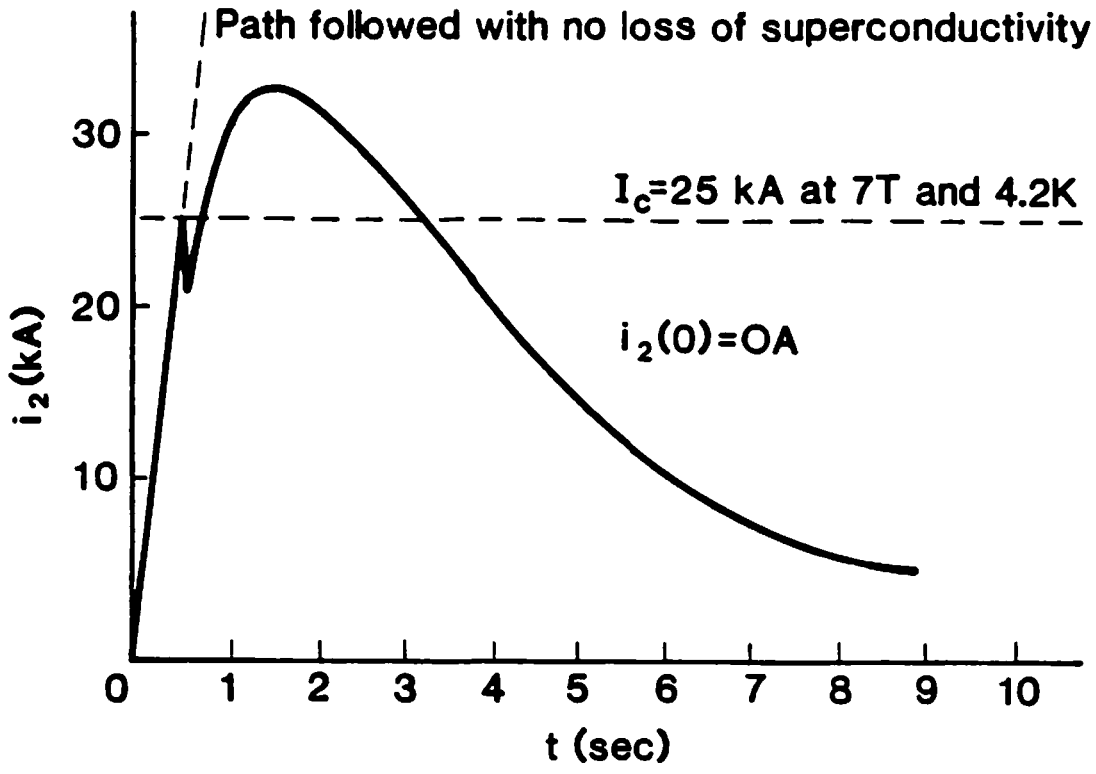

Figure 3.2 Typical profile of induced current as a function of time

where $\theta(\alpha, \beta)$ = factor associated with solenoid geometry.

$$\alpha = \frac{r_0}{r_i} = \frac{369}{272} \approx 1.4$$

$$\beta = \frac{l}{2r_i} = \frac{45}{2(272)} \approx 0.1$$

From the α and β given above (Ref. 3)

$$\theta(1.4, 0.1) \approx 31 \times 10^{-10} H \cdot mm^{-1}$$

and

$$L_2 \approx 272(9)^2(31 \times 10^{-10}) \approx 70\mu H$$

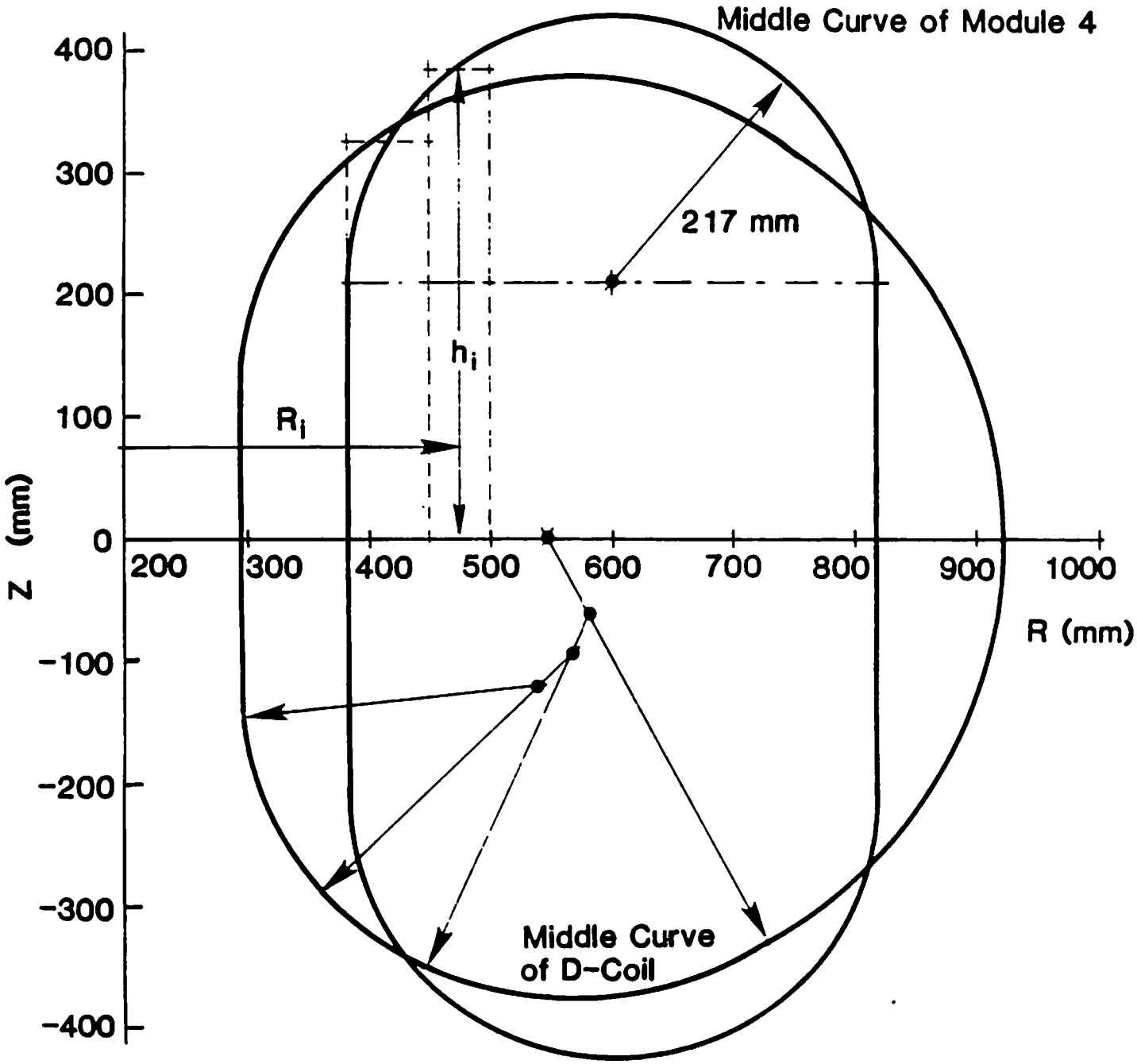

Figure 3.3 Middle curve of Module 4 imposed on middle curve of one TESPE D-coil

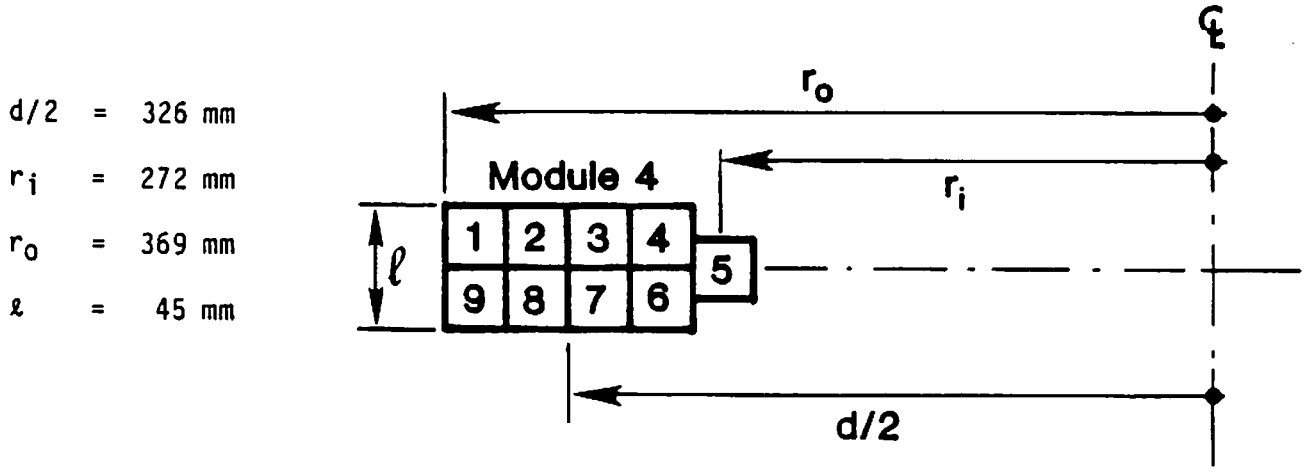

Figure 3.4 Radii associated with a solenoid of middle curve area equal to that of module 4

3.4.2 Circuit Model

The circuit model assumes that Module 4 is the secondary winding of a transformer and that TESPE is the primary winding. It is further assumed that the leads of Module 4 are shorted together and that resistance associated with this short is approximately 1 $\mu\Omega$. See Figure 3.5.

When TESPE discharges, current will decay exponentially according to

$$i = i_0 e^{\frac{-t}{\tau}} \tag{39}$$

where

i	Initial current in TESPE	A
τ	Decay time constant (L/R) of TESPE	s

Thus the differential equation, with solutions given by Eqs. (30) and (31), that describes the behavior of Module 4 as a function of time is

$$L_2 \frac{di_2}{dt} + i_2 R_2 = \frac{M i_0}{\tau} e^{\frac{-t}{\tau}} \tag{40}$$

3.4.3 Temperature Rise

It is assumed that Module 4 behaves like a bare copper cable. That is, the specific heats of the helium, NbTi and stainless steel conduit are neglected. It is further assumed that no heat is transferred away from Module 4. Equating energy input to energy storage, one has

$$\frac{1}{A_{cu}^2}\int_0^\infty i_2^2 dt = \int_{4k}^{T} \frac{\gamma C_p}{\rho} dT \tag{41}$$

where

γ	Mass density of copper	$kg \cdot m^{-3}$
C_p	Specific heat of copper	$J \cdot kg^{-1} \cdot K^{-1}$
ρ	Electrical resistivity of copper	$\Omega \cdot m$

The integral over temperature has the following approximation.

$$\int_{4K}^{T} \frac{\gamma C_p}{\rho} dT = Z(T) - Z(4k) \cong Z(T) \cong Z_0\sqrt{\frac{T}{T_0}} \tag{42}$$

The choice of $Z_0 = 10^{17}\frac{A^2 \cdot s}{m^4}$ at $T_0 = 200$ K is arbitrary and corresponds to a copper RRR≈60. An RRR = 100 changes Z_0 by 10% to $Z_0 = 1.1 \times 10^{17} A^2 \cdot s \cdot m^{-4}$. See Ref. 2.

The current-squared integral can be estimated using Eq. (30) subject to the restriction that $i_2(0) = 0$ A. That is, it is assumed that the currents induced in Module 4 during the charge of TESPE have decayed to zero.

Thus,

$$\frac{1}{A_{cu}^2}\int_0^\infty i_2^2 dt = \frac{1}{A_{cu}^2}\left(\frac{Mi_0}{R_2(\tau - \tau_2)}\right)^2 \int_0^\infty (e^{\frac{-t}{\tau}} - e^{\frac{-t}{\tau_2}})^2 dt \tag{43}$$

$$= \frac{1}{A_{cu}^2}\left(\frac{Mi_0}{R_2(\tau - \tau_2)}\right)^2 \frac{1}{2}\left[\frac{(\tau - \tau_2)^2}{\tau + \tau_2}\right] \tag{44}$$

Equating Eqs. (42) and (44) yields Eq. (29).

3.5 Discussion

Some comments relating to the proposed destructive experiment of the Module 4 coil are given below.

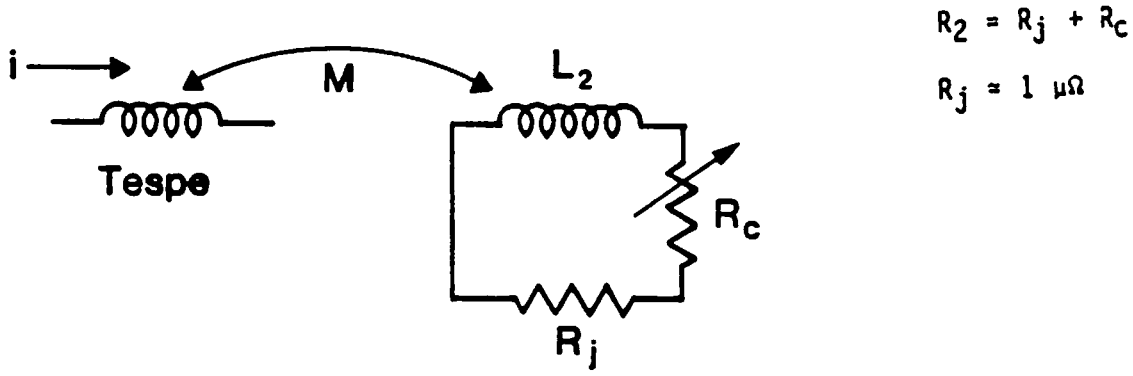

Figure 3.5 Circuit model for Module 4 destructive test

3.5.1 Fit of Module 4 in TESPE

Figure 3.3 superimposes the middle curve of a TESPE D-coil and Module 4. Since the coils have the same approximate size, a fit of the Module 4 coil in one of the gaps between the TESPE D-coils is likely. Current leads of Module 4 will extend approximately 1 meter above the Z = 0 midplane of TESPE.

3.5.2 Current-Lead Terminations

Electrical terminations for the Module 4 current leads have not been completed yet. Figure 3.6 illustrates a possible geometry.

3.5.3 Pressure Relief

Pressure relief must be provided for helium inside of Module 4. This is especially important in a high temperature destructive experiment.

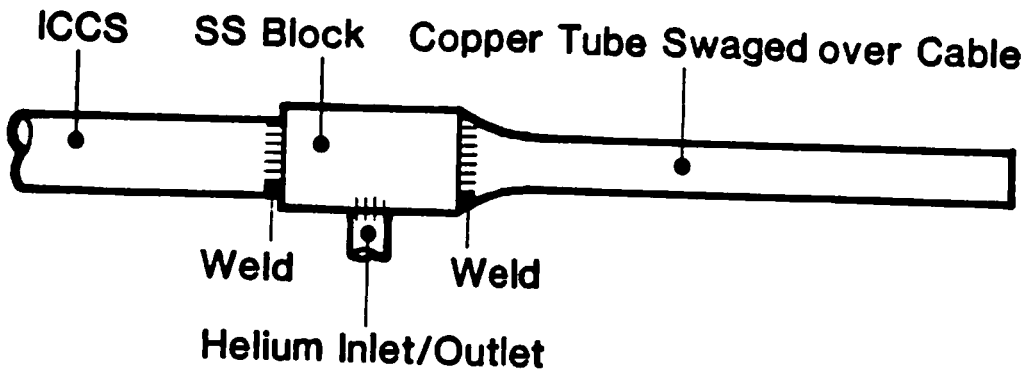

Figure 3.6 Possible geometry for Module 4 current terminations

3.5.4 References

1. Thome, R.J., "Test Module 4, The Football Coil," in Proceedings of the 1980 Conference on Superconducting Magnets, MIT, 1980.
2. Wilson, M.N., Superconducting Magnets, Oxford University Press, London, 1983, p.202.
3. Montgomery, D.B.,Solenoid Magnet Design, Krieger, FL, revised 1980.

3.6 Nomenclature for Section 3

Symbol	Definition	Units
A_{cu}	Copper cross-sectional area perpendicular to axis of 486-strand ICCS	m^2
B	Magnetic field produced by TESPE	T
C_p	Specific heat of copper	$J \cdot kg^{-1} \cdot K^{-1}$
d	Diameter of a circle of area equal to that enclosed by the middle curve of Module 4	m
h	Height of Module 4 middle curve above TESPE midplane measured at a specified radius from the TESPE vertical centerline	m
h_i	Height of Module 4 middle curve at radius R_i	m
i	Current in TESPE D-coils	A
i_0	Maximum current in TESPE D-coils	A
i_2	Current induced in Module 4 due to discharge of TESPE	A
$i_2(0)$	Current in Module 4 at start of TESPE discharge	A
l	Length of Module 4 conductor	m
L_2	Self inductance of Module 4 coil	H
M	Mutual inductance between the TESPE and Module 4 Coils	H
N	Total number of turns in TESPE	
N_t	Number of turns in Module 4	
R	Radius measured from TESPE vertical centerline	m
RRR	Residual resistivity ratio of copper	
R_2	Total resistance (cable and joints) of Module 4	Ω
R_c	Cable resistance of Module 4	Ω
R_i	Radius measured from TESPE vertical centerline to center of rectangle of height h_i and width ΔR_i	m
ΔR_i	Width of ith rectangle used to calculate area inside of middle curve of Module 4	m
R_j	Joint resistance of Module 4	Ω

Symbol	Definition	Units
r_i	Inner radius of fictitious solenoid used to estimate Module 4 self inductance	m
r_0	Outer radius of fictitious solenoid used to estimate Module 4 self inductance	m
t	Time	s
T	Temperature of Module 4 cable	K
T_0	Temperature of Module 4 cable chosen for curve fit (See Reference 2)	K
Z	$\int_{4k}^{T} \frac{\gamma C_2}{\rho} dT$	$A^2 \cdot s \cdot m^{-4}$
Z_0	Value of Z at $T = T_0$	$A^2 \cdot s \cdot m^{-4}$
α	Solenoid outer radius divided by inner radius	
β	Solenoid length divided by inner diameter	
γ	Mass density of copper	$kg \cdot m^{-3}$
θ	Function of α and β used to estimate solenoid self inductance	$H \cdot mm^{-1}$
μ_0	Permeability of free space	$H \cdot m_{-1}$
ρ	Electrical resistivity of copper	$\Omega \cdot m$
τ	Current decay time constant of TESPE	s
τ_2	Current decay time constant of Module 4	s
ϕ	Flux linking the middle curve of Module 4	Wb

4 P-MAX Simulation Analysis With SPICE

J.R. Hale

4.1 Introduction

The coil designated as P-Max, shown schematically in Figure 4.1, was designed to meet the need to measure peak pressure in an ICCS (bundle-in-tube) conductor. Miller, Dresner and Lue [2] have measured the peak pressure (P_{max}) in an ICCS conductor under conditions of simultaneous quench. This coil was built to evaluate P_{max} in a system in which the quench is initiated at some point and then propagates through the conductor at its "normalizing" speed. Dresner [3] has published his predictions for such a system. The overriding need to evaluate P_{max} arises because advanced superconductors will have ever-increasing current densities creating increased competition for space among the three conductor components – superconductor, copper stabilizer, and liquid helium.

P-Max was wound using a 27-strand bronze-matrix Nb_3Sn stainless-steel-sheathed ICCS conductor. The winding consisted of two 75 m lengths of the conductor that were wound two-in-hand. Except for the short "front" lengths wound on a 2.875-inch diameter mandrel, the bulk of the two conductor lengths was wound as a six-layer coil on a 5-inch- diameter mandrel. The objective was to determine peak pressure on quench. Consequently 10,000 psi pressure transducers were attached at the termination of each of the conductors, near its small inner coil. The inner coils, coupled to a heater, were used as the quench initiation point.

P-Max was fabricated using an insulate/wind/react/epoxy pot processing sequence. The ceramic insulation used was not rugged enough to withstand the wind/react sequence without use of a binder. The coil thus had conductor-to-conductor and conductor-to-ground electrical shorts.

---

[2]Miller, J.R., Dresner, L., Lue, J.W., Shen, S.S., Yeh, H.T.. Pressure rise during the quench of a superconducting magnet using internally cooled conductors, Proc. 8th International Cryogenic Engineering Conference, 321, (1980)

[3]Dresner,L., Quench Energies of Potted Magnets, *IEEE Trans. Mag.* MAG-21, 392-395, (1985).

A series of measurements was carried out at KfK in which a propagating quench was initiated at increasing values of transport current, up to 1800 A. Pressure increases up to 5.5 atm were recorded on top of a 3 atm base pressure at an 1800 A total current through the two conductors in parallel. At 2000 A there was no pressure increase. The base pressure actually dropped to one atm. The coil is no longer viable, since it cannot be pressurized.

Subsequent to a review of the results of an extensive series of voltage measurements, and discussions with the designers and technicians who knew the coil firsthand, the following preliminary conclusions were formulated:

- Conductors from inner coils A and B are shorted together, and to the case, at the point where they pass through a notch in the stainless outer coil spool.
- The two outermost layers of coil B are shorted together at the upper end. That is, by virtue of the manner in which they are wound, those two layers are, in effect, in parallel with a resistive short.
- Voltage tap 14 (and its redundant colleague, 16), does not form a pair with tap 13 on inner coil B, but rather, is connected to the input of the inner coil *A*.

These three features are shown schematically in Figure 4.2.

The analysis which follows leads to these two conclusions: 1) little damage would likely be done by current flowing through the shorts during slow magnet charging; 2) during a "dump" from an initial current of several hundred amperes, the heating within the shorts would likely be sufficient to damage the stainless steel sheath.

4.2 Preliminary Circuit Model for SPICE

A copy of the comprehensive circuit analysis program, SPICE2[4], was made available on our DEC VAX-780 computer. A detailed circuit description

[4]Developed at the University of California, Berkeley, by Dr. Lawrence Nagel, and others.

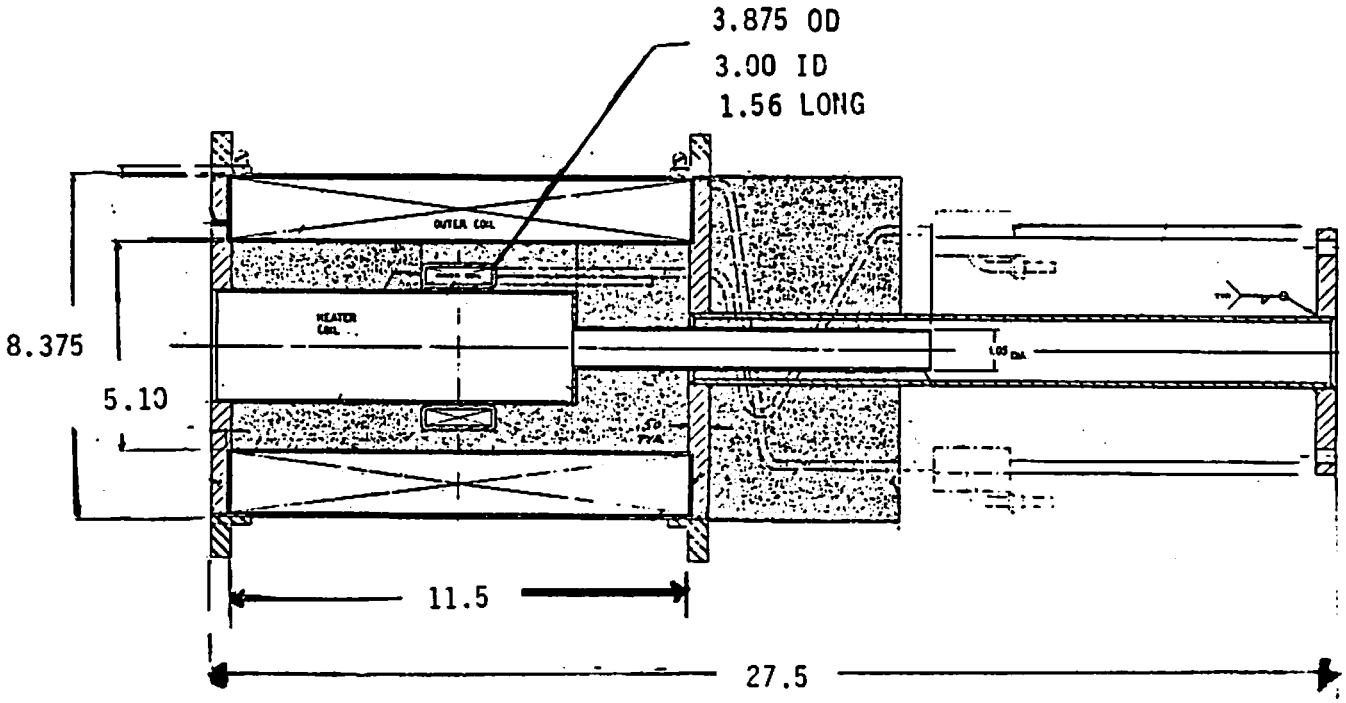

Figure 4.1 Schematic Illustration of the P-Max Coil

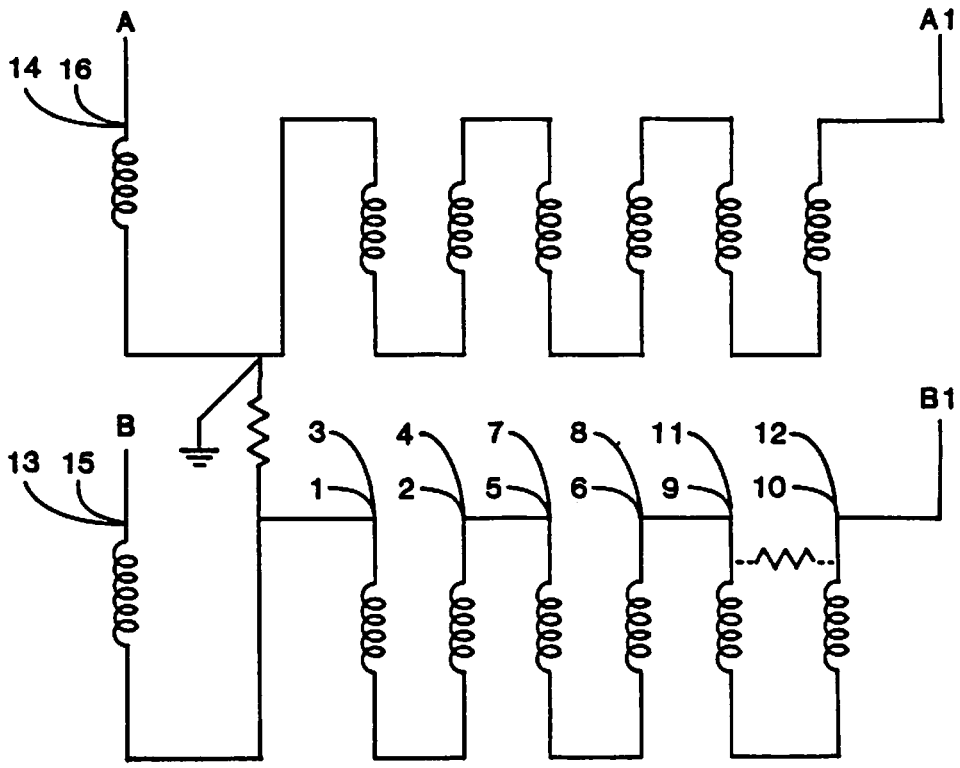

Figure 4.2 Simplified Schematic Circuit of P-MAX

of the P-MAX coil system was written in a format appropriate for input to this program, including computed values of inductance for each layer of each of the coils, A and B, as well as the array of mutual inductances between each pair of layers. The output from the program enables us to get some idea of how much current might flow through various of the shorts believed to exist.

For purposes of analysis, the coil system was considered to comprise fourteen separate coils. That is, each of the seven layers of set A and of set B was taken to be a separate entity. The inductance matrix of this system of fourteen coils was calculated, and the results used as input to the circuit analysis program. For this analysis, coils A and B were considered to be connected in parallel. For several initial runs, provision was made for shorts between every layer in coil A and the corresponding layer in coil B. But, the SPICE program failed with a floating-point overflow error whenever the effective short resistance across the two outer layers of B was less than 0.2 ohms. On the other hand, runs were successful with a value as small as 0.001 ohm if only the outer layer was shorted. So, several cases were run

with this configuration, and the next part of the discussion outlines those results.

To simulate a worst case, the input voltage was raised to seven volts[5] in 0.1 seconds, and then, once the current reached 3000 amperes, was reduced to 1.35 volts, which is enough to overcome the IR drop in the simulated current leads.[6].

Twelve cases were run, with different values of equivalent short resistance. The following features were noted:

- Turn-to-turn shorts from set A to set B have little effect on the distribution of current, yielding and A - B unbalance of less than 2 amperes in the "worst case" run, and the unbalance disappears after 200 ms.

- The greatest potential source of unintended current excursions is at the outer layer of coil B.

Inasmuch as this was not the most realistic case, that is, only the outer layer was in parallel with the alleged short, other details of these results are not relevant.

Next, an attempt was made to simulate a sudden switching off of the power supply, with the application of a dump resistor across the coil terminals, because it was felt that during such events, the current in a short could be even larger than it would be during magnet charging. However, here again, SPICE failed with a "floating overflow." For this reason, the circuit model was simplified.

4.3 Refined Circuit Model

In hopes of extending the versatility of the circuit simulation, it was determined that by eliminating the A–B shorts from the model circuit, which the preliminary analysis had shown would not appreciably affect the results for the outer two layers, all incidence of floating-point errors was eliminated. Thus, the simulation could be made more realistic by placing the short of greatest interest in parallel with the outer two layers. Furthermore, dump

[5]The maximum available from the power supply at KfK.

[6]taken to be a total of 10 meters of cable, comprising the equivalent of four 4/0 cables in parallel. This was later changed to 10 feet, which was a more realistic length

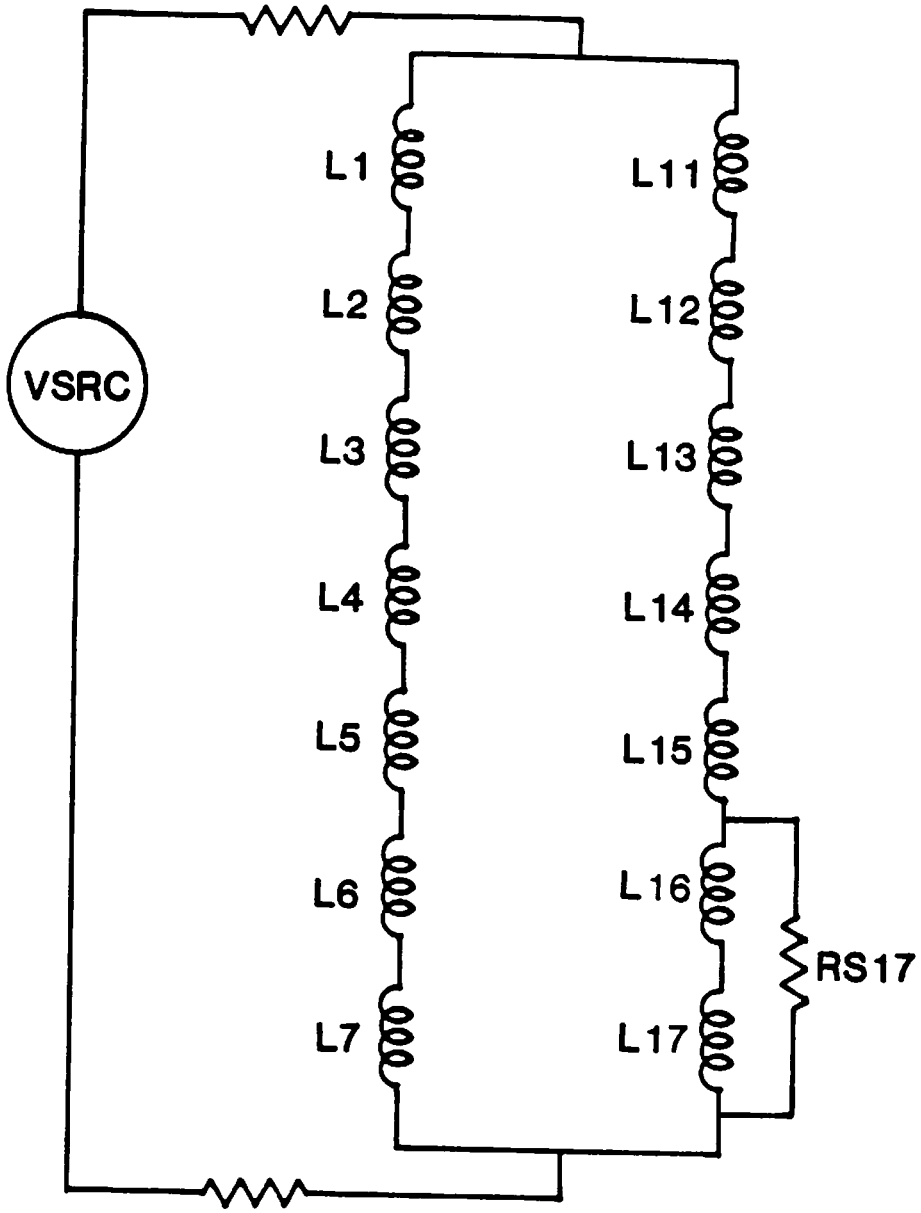

Figure 4.3 Final Circuit Model Diagram for SPICE

simulations, too, could be carried out without unleashing floating-point errors. Figure 4.3 shows the redesigned circuit drawn for SPICE input, and Figure 4.4 at the end of the report depicts a typical energizing scenario, details of which appear in a separate section of graph descriptions.

Once the circuit model was functioning satisfactorily, the question of whether it had within it a reasonable value for the resistance of the alleged short grew more pressing, inasmuch as the next scenario to undergo simulation would be a series of dumps. Would the heat generated in such a short during a dump cause significant heating of the sheath?

An estimate of the resistance was carried out by the following computation,

$$R_s = \frac{\rho L}{A}$$

with the following values:

- Resistivity, $\rho = 120\ \mu\Omega$-cm, a value typical for Hastalloy.
- "Length", $L = 0.122$ cm, twice the thickness of the sheath.
- Area, $A = 10^{-2}$ cm^2, that is, 1 square millimeter.

This yielded a value of $R_s = 1.5$ mΩ, which lent credibility to the value of 1 mΩ that had been used as a "typical" short resistance for many of the previous runs, and subsequently for all of the dump simulations.

4.4 Dump Simulations and Analysis

The intent of the P-MAX experiment was to measure the peak pressure rise in the ICCS during quench. In practice, a quench was simulated by heating the innermost layers of both coils, A and B, which led to an increasing voltage at the terminals, and eventually, the quench detection circuitry caused the main current breaker to open at some preset voltage level.

To simulate this scenario, it was necessary to alter the model and the SPICE input file slightly. Figure 4.4 shows the circuit as modified for dump simulation. A small resistance, calculated from cable specification data to be 0.1 mΩ, was put in series with each inner layer to represent the normal-state resistance of the quenched turns. Initial conditions could be specified to ensure that any desired current would be flowing at $t = 0$, when the breaker opening was set to occur.

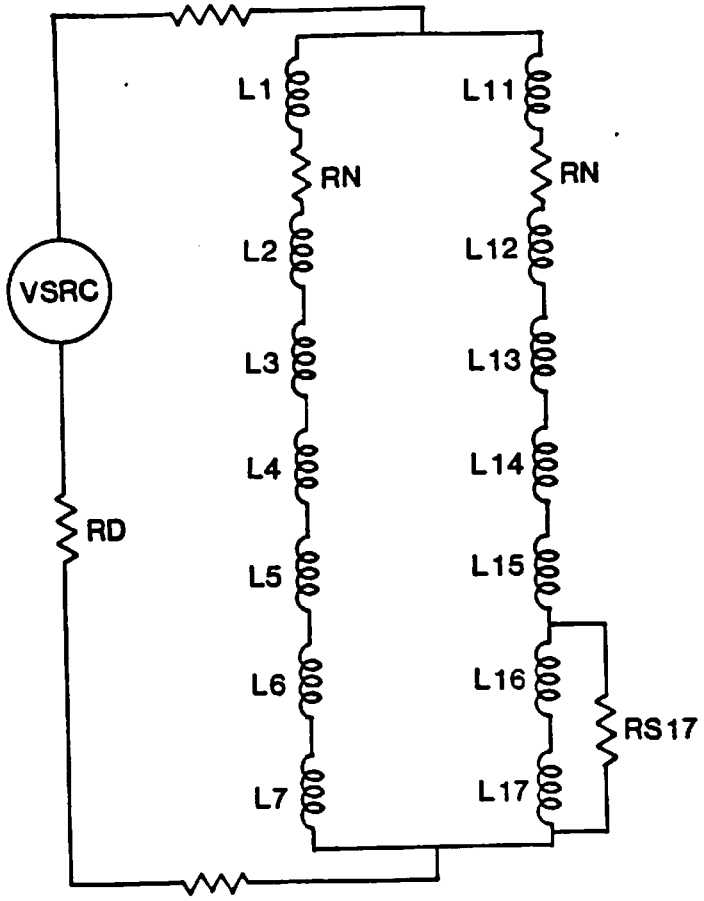

Figure 4.4 Circuit Modified for Dump Simulation

4.4.1 Computation Strategy

The goal of the dump simulations was to make a rough estimate of whether the stainless steel sheath could be heated to its melting point as a result of current flow through a small shorted contact area. The governing equation was taken to be

$$\int_{T_i}^{T_f} \frac{\gamma c_p}{\rho} dT = \frac{1}{A^2} \int_0^\infty I^2 dt$$

The first step toward the solution was to work out the left side of the equation for the sheath. A value of 7.8 g/cm^3 was assigned to the density, γ, and the electrical resistivity, ρ, was found to be relatively insensitive to temperature and was assigned a value of 120 $\mu\Omega$-cm.

Next, a reference work[7] was located, in which the specific heat of type 316 stainless steel was plotted over the temperature range 0–1300 K. The

[7]Parker, D. and Bernstein, I.M. *Handbook of Stainless Steels*, McGraw-Hill, 1977, pp.19-26.

application of a planimeter to this curve yielded a number of coordinate pairs, T vs $\int_{T_i}^{T} c_p dT$. This set of coordinate pairs was given as input to a cubic spline interpolation program, running on a DEC PRO/350 (PDP-11/23+) personal computer, which gave as output 100 coordinate pairs. The abscissae were multiplied by γ/ρ, producing a file of coordinate pairs suitable for plotting, the results of which appear in the next section.

The right side of the equation was computed in a similar manner, making use of current transients computed with SPICE. Inasmuch as the effective contact area (A in the equation) was unknown, the integral was evaluated for several values of area, ranging from 10^{-2} to 6.25 x 10^{-2} cm^2. The transient analysis by SPICE showed that the current through the short died away within about 2 seconds, so that the curves of I^2, for three values of initial current, were integrated with the planimeter from $t = 0$ to $t = 2$. Finally, three coordinate pairs, $\frac{1}{A^2}\int_0^2 I^2 dt$ vs I_0, for each of four values of A were put through the cubic spline program, yielding input for the plotting routine.

To make use of these results to judge whether the stainless steel sheath might be damaged during a dump, one proceeds as follows. First, look up on one of the figures 4.10, 4.11, or 4.12 the ordinate corresponding to the initial current in question. For example, take 750 amperes on Figure 4.11, the result being about 4 x 10^7 A^2-s/cm^4. Second, from Figure 4.13, one reads that the temperature of the sheath might reach 1200 K. As another example, consider the same initial current, but a contact area, $A = 10^{-2}$ cm^2. Figure 4.10 yields a value of 1.2 x 10^9, which is way off scale on Figure 4.13.

The conclusion is that during a dump from an initial current of several hundred amperes, the heating at the contact area is likely to severely damage the stainless steel sheath.

Having gone through this exercise for the dump scenario, it seemed worthwhile to backtrack to the slow-energize scenario, to judge whether in that case, too, the sheath could be damaged. Figure 4.13 shows I^2 vs. t (ref. Figure 4.5) for energizing to full current. The value of $\int_0^{16} I^2 dt$ is a factor of 75 less than the case of a dump from full current. Furthermore, during the slow energizing, active cooling would be taking place. One can be reasonably certain, then, that for the conditions stated herein, little damage would be done by current in the short during magnet charging.

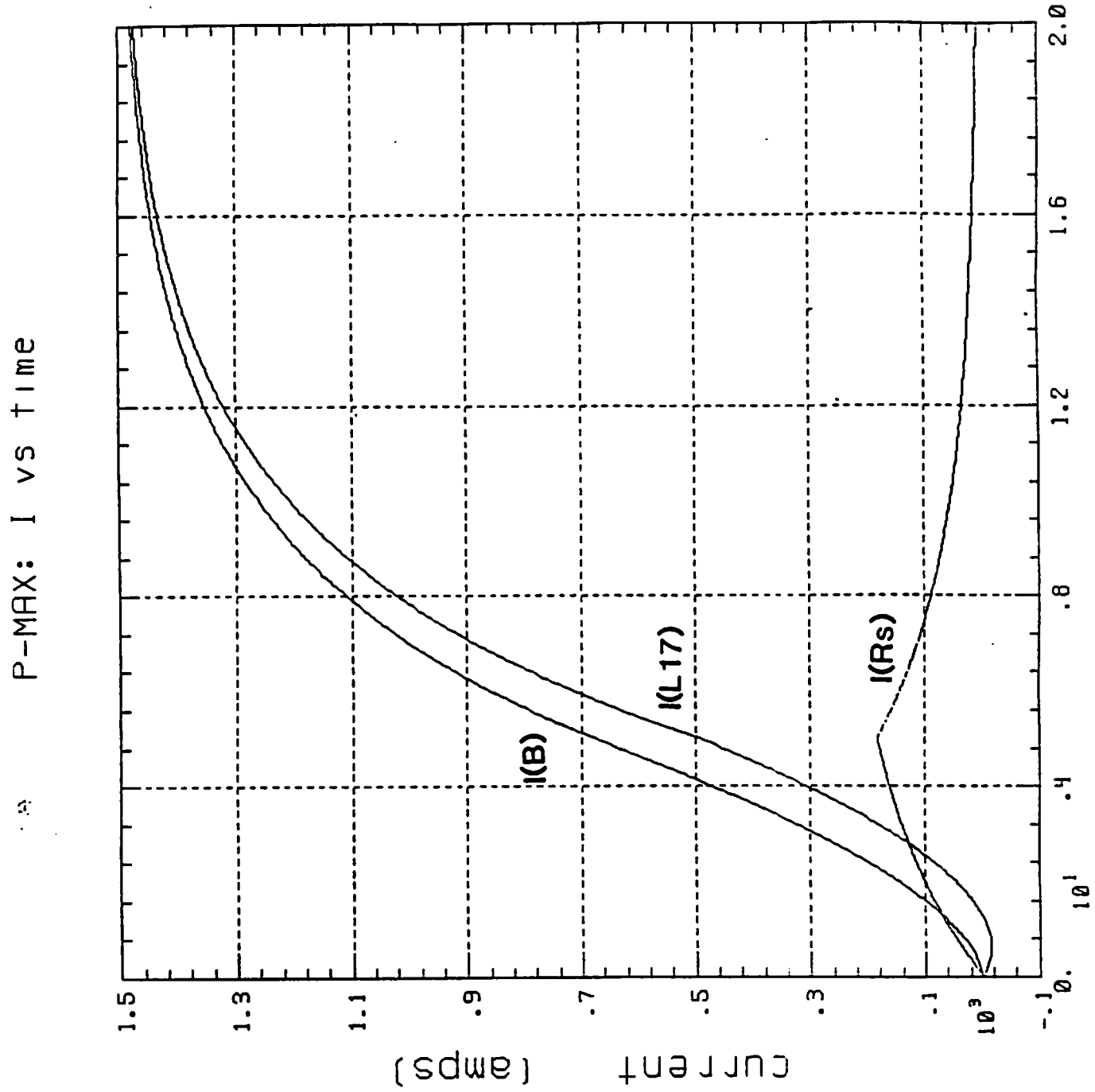

Figure 4.5 This plot shows the current in coil B, in the outer two layers—labeled I(L 17)—and in the short during energizing at 0.903 volts for 5 seconds. Note the modest negative swing of the current in the outer two layers. The current in the short begins to decay as soon as the 5 second rise-time of the input voltage has past.

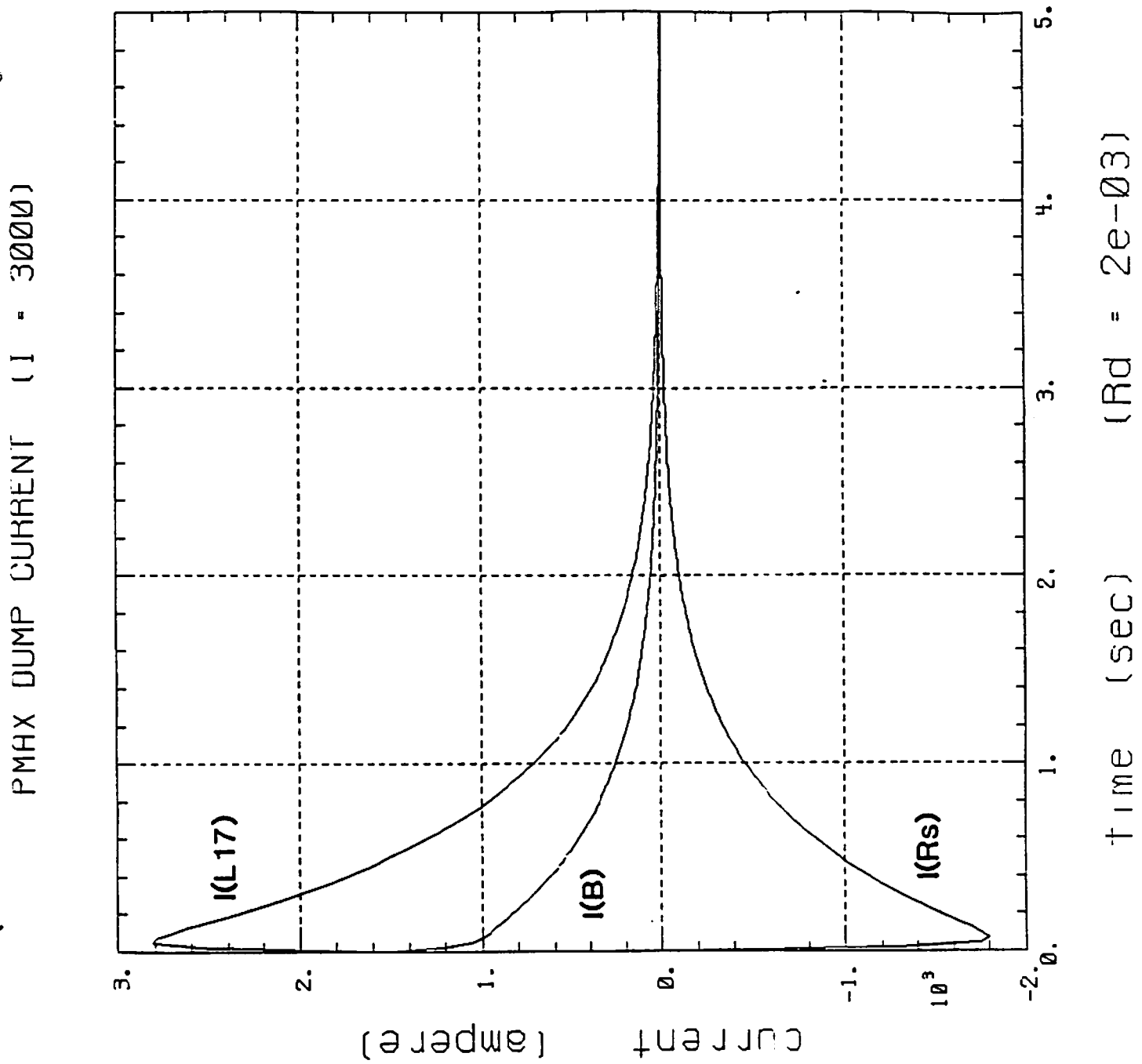

Figure 4.6 This is a typical dump scenario, this case depicting current flow in the same three locations as in Figure 4.5 The initial current was 3000 amperes, and the dump resistor for this run was 2 mΩ.

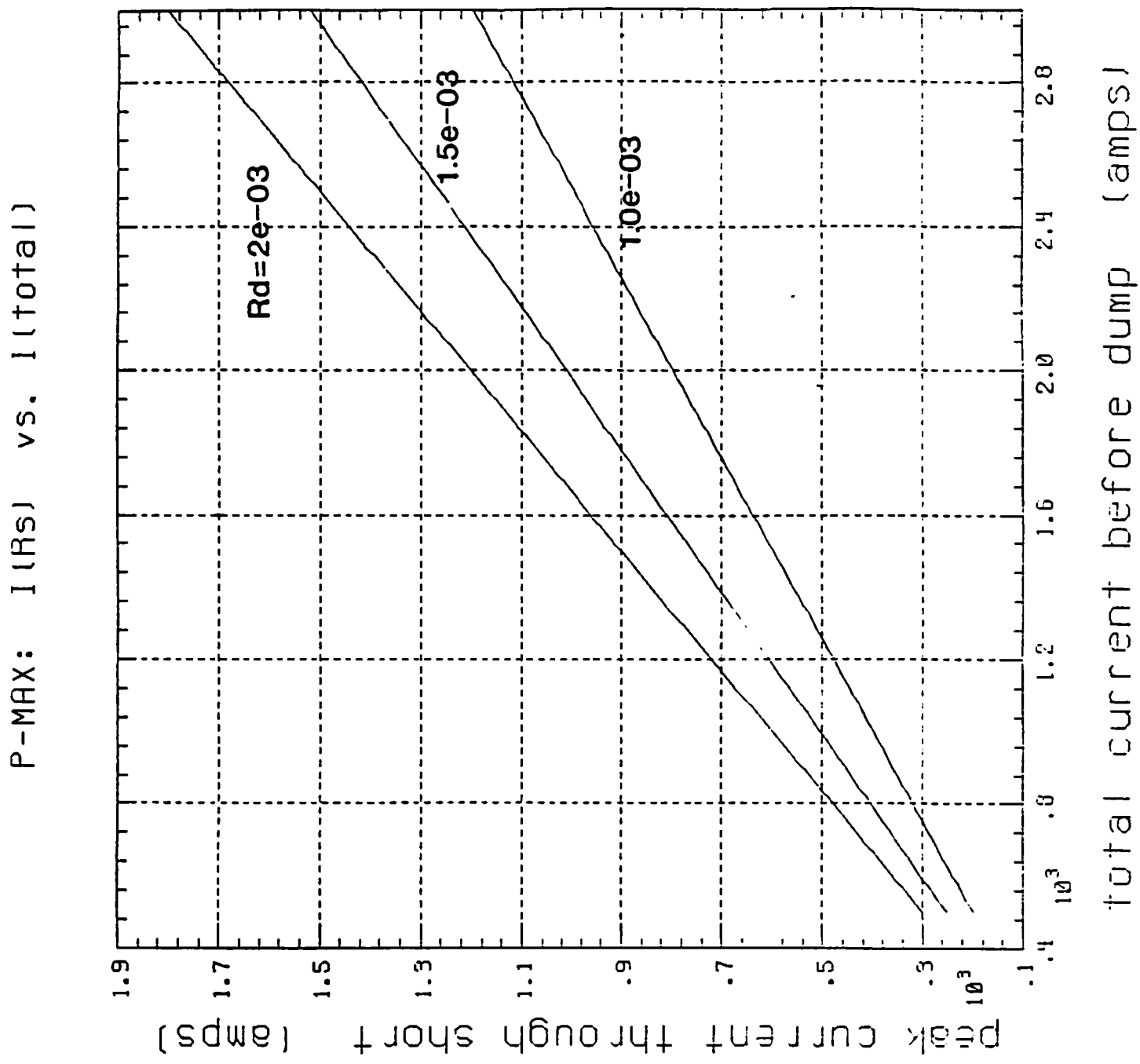

Figure 4.7 The peak current, I_p, through the short as a function of initial current, I_0, is plotted here, for three values of dump resistance. The actual value of R_d is believed to fall somewhere within the range depicted here.

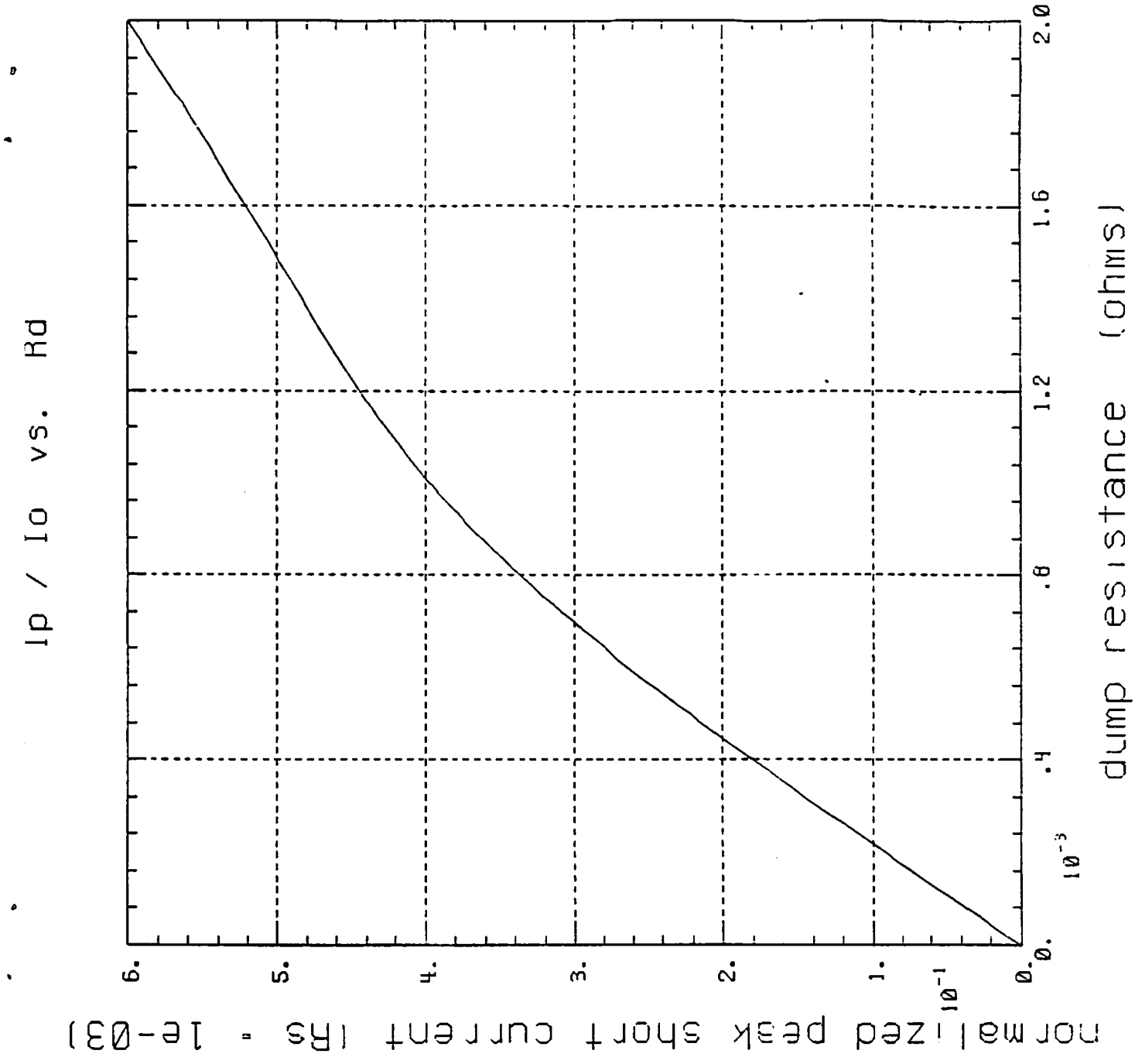

Figure 4.8 Another view of the data in Figure 4.7; the peak current is normalized to the corresponding value of initial current, yielding a plot of I_p/I_0 vs. R_d.

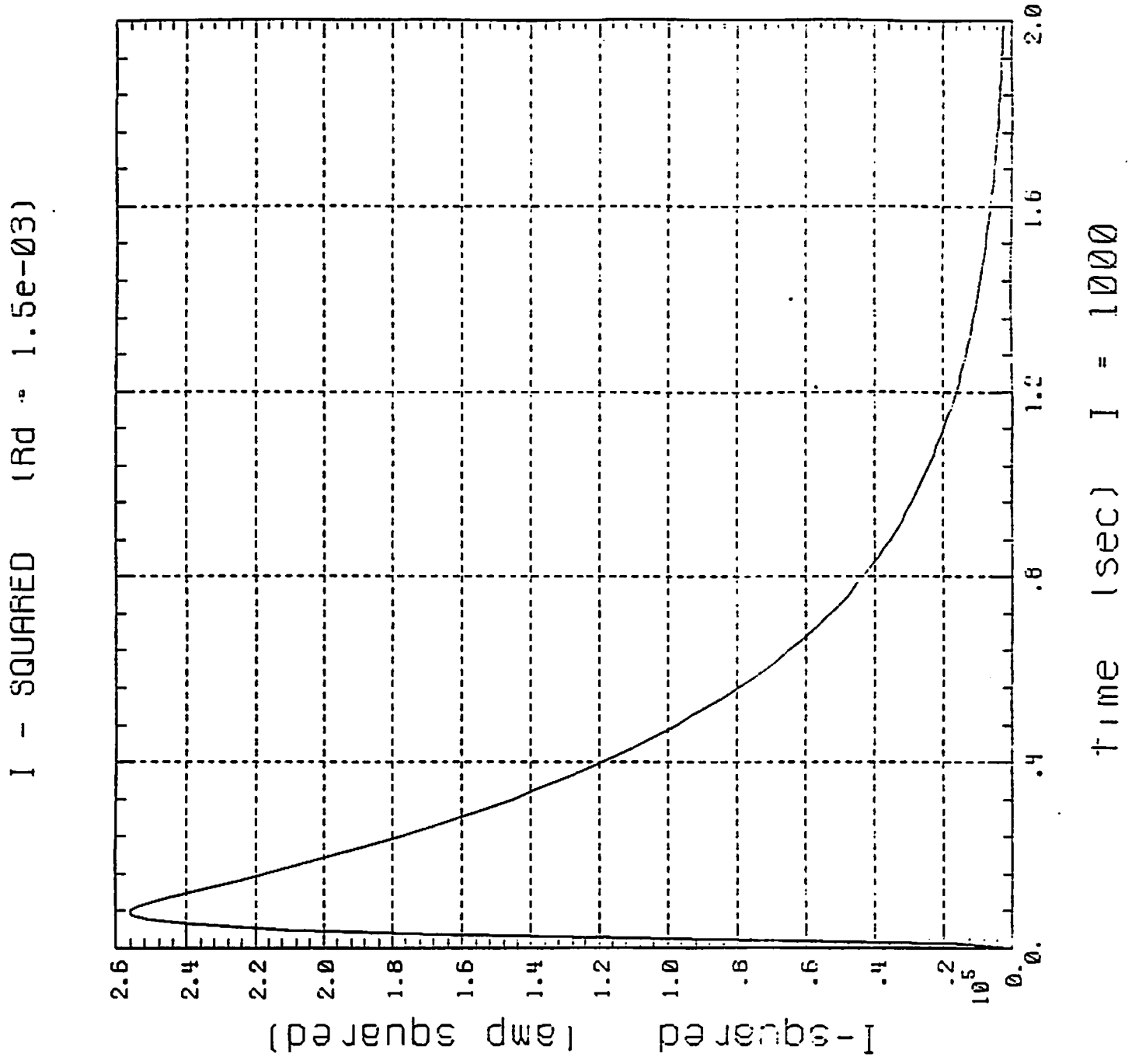

Figure 4.9 Here is a typical graph of I^2 as a function of time, this one for the case of $I_0 = 3000$ and $R_d = 1.5$ mΩ. Note that by $t = 2$, further contributions to $\int_0^t I^2 dt$ are very small indeed.

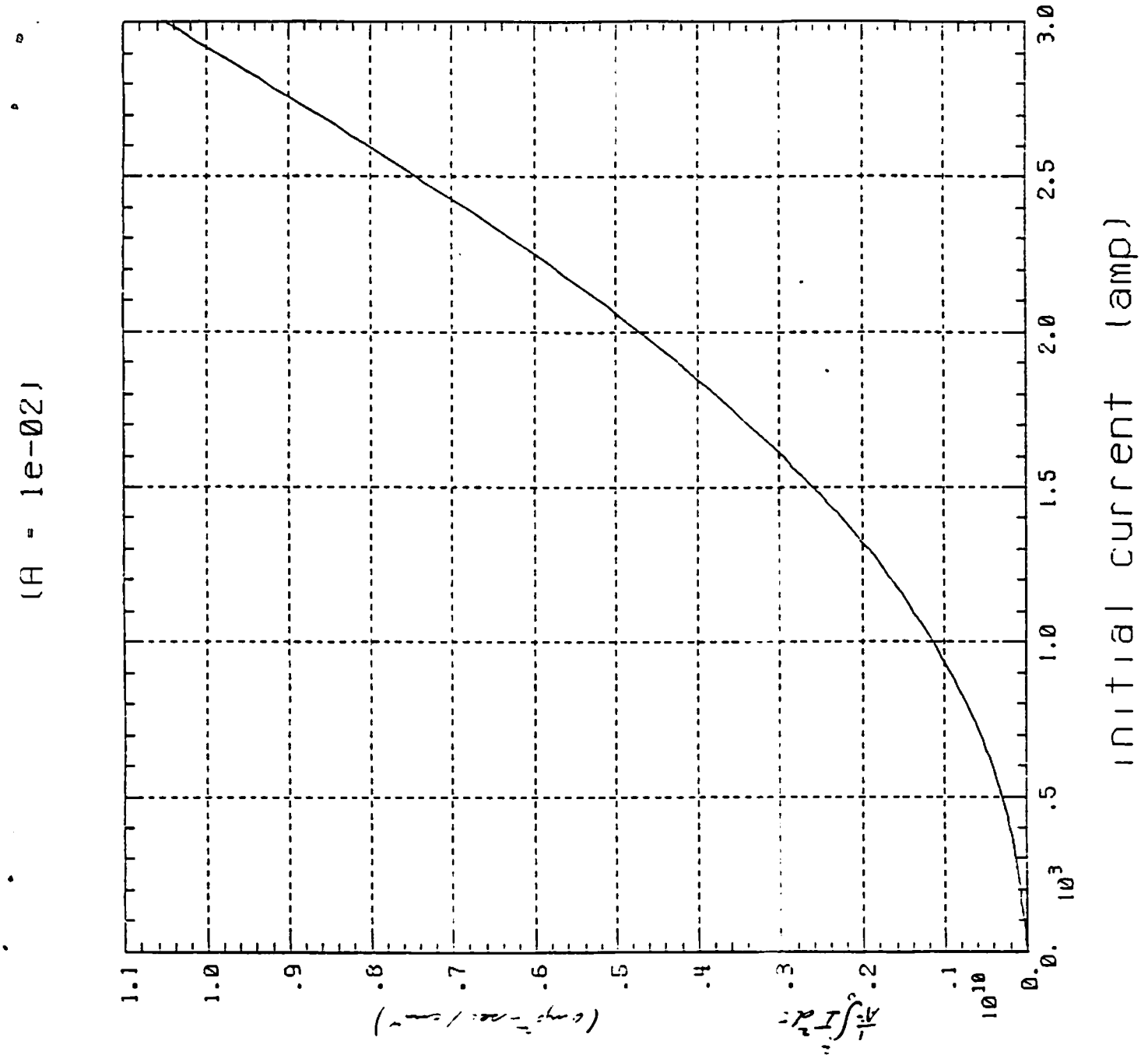

Figures 4.10, 4.11, 4.12 These curves show the value of the right side of the equation in section 4.1, as a function of initial current, for three values of contact area, A.

(A = 4e-02)

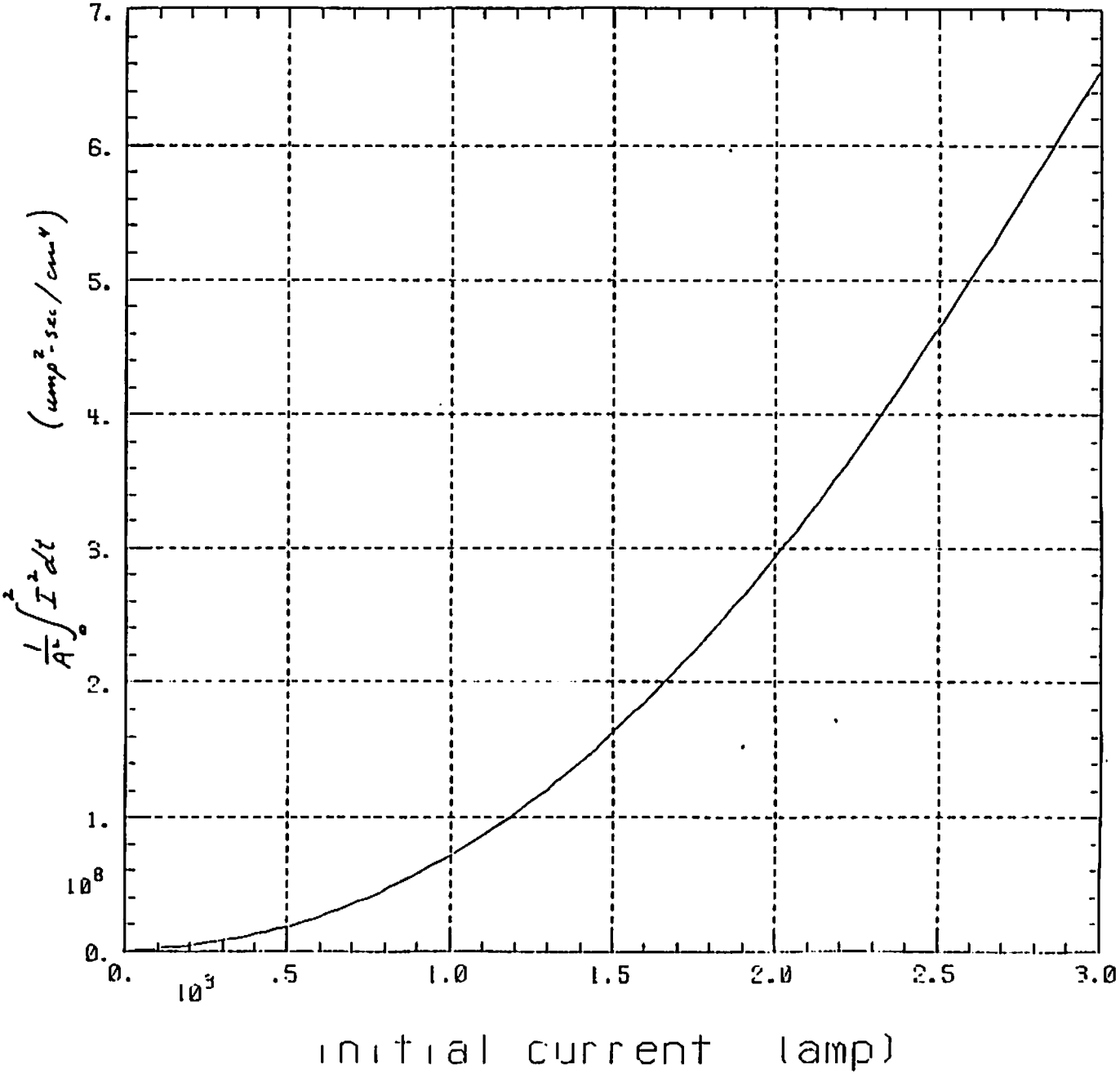
7.
6.
5.
4.
3.
2.
1.
10^8
0.
0.
10^3
.5
1.0
1.5
2.0
2.5
3.0
(amp^2-sec/cm^4)
1/A^2 ∫ I^2 dt
initial current (amp)

(A = 6.25e-02)

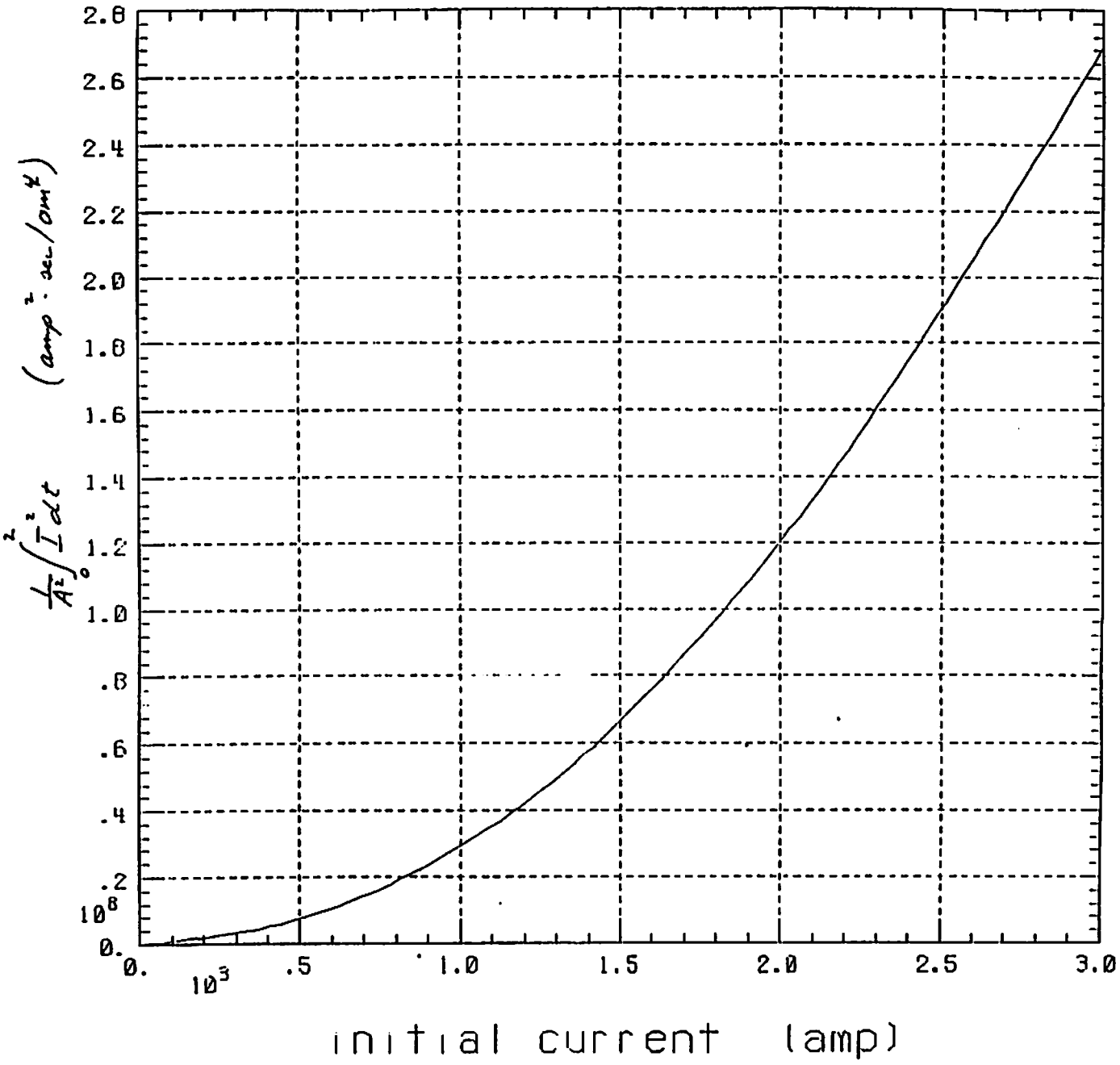
2.8
2.6
2.4
2.2
2.0
1.8
1.6
1.4
1.2
1.0
.8
.6
.4
.2
10^8
0.
0.
10^3
.5
1.0
1.5
2.0
2.5
3.0
$\frac{1}{A^2}\int_0^2 I^2 dt$ (amp^2 · sec/ohm^2)
initial current (amp)

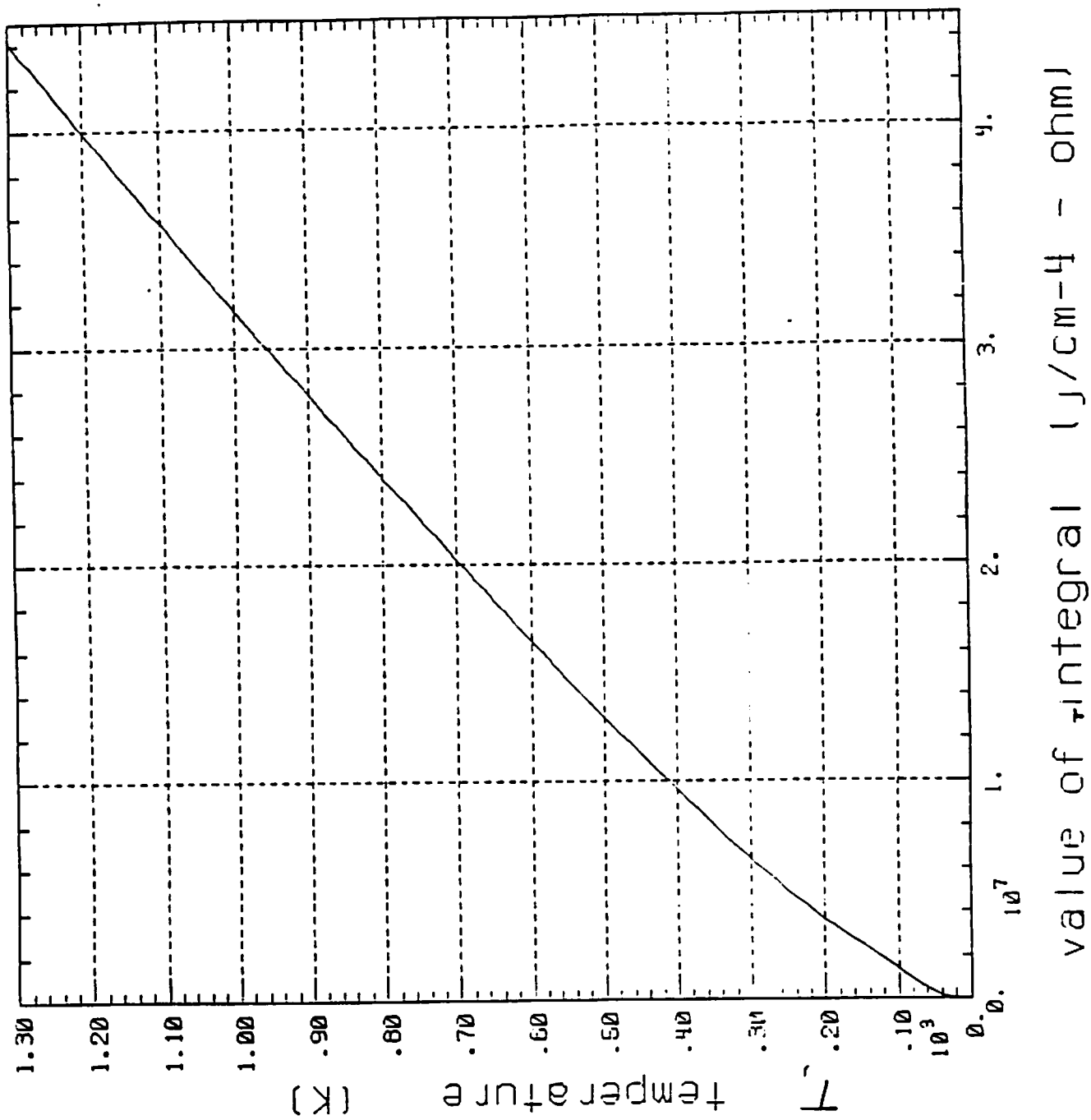

Figure 4.13 The sheath temperature is depicted here as a function of the value of the left side of the equation in section 4.1, $\int_{T_1}^{T_f} \frac{\gamma C_p}{\rho} dT$.

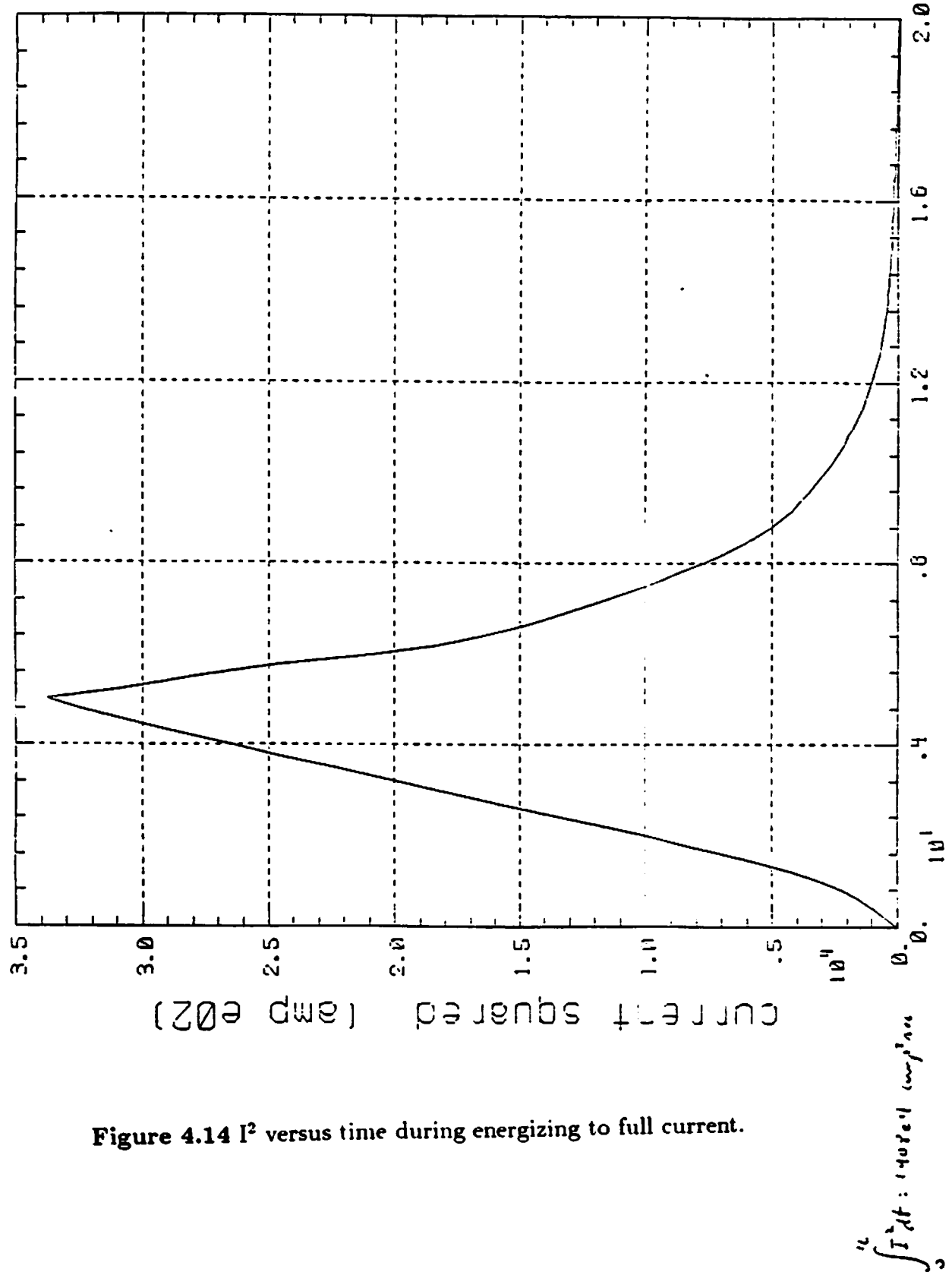

Figure 4.14 I^2 versus time during energizing to full current.

5 Publications

The following publication was prepared in FY86 and reports work supported in part by this contract.

- Thome, R.J., Czirr, J.B., Schultz, J.H., *Survey of Selected Manet Failures and Accidents* presented at the American Nuclear Society, Topical Conference on Fusion Problems, Reno, June 1986.